CZECH TECHNICAL UNIVERSITY IN PRAGUE

Faculty of Nuclear Science and Physical Engineering

Influence of Energy Scale Imperfections on Neutrino Mass Sensitivity in the KATRIN Experiment

Diploma Thesis

Author: Jaromír Kašpar

Supervisor: Ing. Antonín Špalek, CSc.

Supervisor: RNDr. Miloš Ryšavý, CSc.

2003

Prohlášení

Prohlašuji, že jsem svou diplomovou práci vypracoval samostatně a použil jsem pouze podklady uvedené v přiloženém seznamu.

Nemám závažný důvod proti užití tohoto školního díla ve smyslu § 60 Zákona č. 121/2000 Sb., o právu autorském, o právech souvisejících s právem autorským a o změně některých zákonů (autorský zákon).

V Praze dne 21. 1. 2003

Abstract

The KATRIN experiment is a model independent direct measurement of the neutrino mass by means of beta ray spectroscopy. We have studied influence of possible imperfections of the spectrometer energy scale on the neutrino mass sensitivity. In particular, we have examined both static and time dependent variants of an energy bias and an improper slope of the calibration line.

Abstrakt

KATRIN je modelově nezávislý experiment umožňující přímé měření hmotnosti neutrina spektroskopií záření beta. Zkoumali jsme poruchy energetické osy spektrometru ve vztahu k citlivosti experimentu na hmotu neutrina. Zaměřili jsme se na vychýlenou nulu stupnice a nesprávný sklon kalibrační přímky a to jak na konstantní, tak i časově proměnný případ.

Contents

Preface

One of the most fundamental tasks of particle physics is definitely the determination of the neutrino mass. This can be measured by beta ray spectroscopy in very natural and model independent way. The Karlsruhe Tritium Neutrino (KATRIN) experiment is a proposed next-generation tritium beta decay experiment, which is designed to perform a high precision direct measurement of the neutrino mass with sub-eV sensitivity. Leading systematic uncertainities in the experiment include instabilities and inhomogenities of electrostatic fields. A special case of these are energy scale imperfections.

Therefore, the aim of this work is to investigate how the possible energy scale imperfections influence neutrino mass sensitivity in the KATRIN experiment.

This paper is organized as follows. Basic ideas and concepts of the KATRIN experiment are summed up in the first part of this work. The second section introduces our numerical model of the experiment, shows that the model is accurate and consistent, and finally applies the model to investigation of energy scale imperfections and their influence on neutrino mass sensitivity.

I am very grateful to both my supervisors, Miloš Ryšavý and Antonín Špalek for their patience and encouragement throughout the writing of this diploma thesis. Also I would like to thank to Otokar Dragoun, Christian Weinheimer, Klaus Eitel and Nikita Titov for their helpful ideas and valuable conversations, that significantly influenced this work.

1 KATRIN

1.1 Overview

The Karlsruhe Tritium Neutrino (KATRIN) experiment [1, 2] is a next-generation tritium beta decay experiment with a sensitivity to sub-eV neutrino masses. The sensitivity on the electron neutrino is expected to be $m_\nu \leq 0.35\,\mathrm{eV}$ (90 % c.l.), which is about one order of magnitude better than the sensitivity of current experiments. The equipment used in the KATRIN experiment can be subdivided into five functional units:

- two molecular tritium sources: a high luminosity windowless gaseous tritium source (WGTS) delivering 10^{10} beta decay electrons per second and a quench condensed tritium source (QCTS)
- an active differential pumping section at the rear and front side of the WGTS to reduce the flow of tritium molecules from the WGTS into the residual system
- a cryotrapping section with Ar-frost to eliminate the remaining flow of tritium molecules and to keep the spectrometer essentially tritium-free
- a system of two electrostatic filters consisting of a pre-spectrometer at fixed retarding potential, which filters out low energy beta decay electrons and a large volume main spectrometer,which analyses the beta electrons close to the tritium endpoint at 18.6 keV
- a segmented semiconductor detector or bolometer array to count the beta electrons transmitted through the electrostatic filters

1.2 Tritium sources

1.2.1 Windowless gaseous tritium source

The main principle of the WGTS [3] is adiabatic transportation of beta decay electrons from a long tube, which is filled with tritium and is differentially pumped out on both ends of the tube with injection of tritium at the middle of it. The WGTS will be [1, 4] a 10 m long cylindrical tube of 90 mm diameter, filled with molecular tritium gas of high purity ($> 95\,\%$). The tritium gas density at the middle of the tube will be $10^{15}\,\mathrm{molecules\,cm^{-3}}$. A working temperature around 30 K stabilized to ± 0.2 degrees will keep the source strength constant. The tritium tube will be placed inside a chain of superconducting solenoids of 1 m length each, generating homogenous magnetic field of $B_S = 3.6\,\mathrm{T}$.

The main advantages of the WGTS are as follows [2, 3]:

- investigation of the tritium beta spectrum with the highest possible energy resolution, limited only by the spectrum of final state vibrational and rotational excitations of the daughter molecule $(^3\mathrm{HeT})^+$
- guaranteed homogenity of density over the whole source cross section
- use of a high specific activity
- no pertubating solid state effects
- a possibility to measure the energy loss spectrum of electron inelastic scattering in the source

On the other side, the possible problems are:

- stability of the source strength
- magnetic trapping of charged particles in the local magnetic field minima between the solenoids of the source
- tritium penetration to the spectrometer volume

1.2.2 Quench condensed tritium source

The QCTS is formed by a thin film of molecular tritium frozen on a graphite substrate. The QCTS suffers from the self charging effect, which is the cause of systematic uncertainties. These are, on the other side, independent on WGTS systematic effects, so a measurement with the QCTS could provide an effective way of systematics study. The self charging is also the limiting factor of luminosity.

1.2.3 Operation modes

Apart from the standard tritium measurements, other specific modes of tritium sources operation may be required. All the modes are listed below [2]:

- standard operation of the WGTS, i.e. the long-term measurement of the tritium beta spectrum
- standard operation of the WGTS in the ToF mode (for details see section 1.4.2), i.e. the mode focused on systematics study and background investigations
- the WGTS work function measurement with ^{4}He, i.e. high precision electron spectroscopy of a very sharp electron line at 35 eV originating from an autoionization state of ^{4}He
- the QCTS operation
- energy loss measurements of 18.6 keV electrons in the WGTS, i.e. the mode providing information on energy loss spectrum, as well as the total inelastic

cross section of electrons at this energy. The cross section uncertainty could be the dominating systematic error in the KATRIN measurements

- source system cleaning by bake out, i.e. the mode removing tritium and argon (see the next section for detailes) from the inner surfaces. Temperature of 550–600 K will be required

- energy calibration with gaseous ^{83m}Kr. The calibration lines of our interest are K-32 conversion line at the electron energy of 17.8 keV, the L-32 lines at 30.4 keV and the N-32 lines at 32.1 keV. Estimated krypton-tritium ratio of the order of 10^{-6} and the WGTS temperature of 100–150 K will be used in this mode

1.3 Differential and cryogenic pumping, electron transport system

The electron transport system guides beta decay electrons to spectrometr, which has to be kept tritium free mostly for background reasons. The tritium flow into the spectrometer should be smaller than 2.7×10^6 molecules s^{-1} to limit the increase of background to 1 mHz. See [1, 4] for details.

The transport system consists of 1 m long tube elements, which are tilted by 20° with respect to each other. At the rear and the front end of the WGTS, the tubes are placed in superconducting solenoids ($B = 3.6$ T) and are kept at the temperature of 30 K. Their diameter is proposed to be 90 mm. At the gaps between the transport solenoids there are located the pumping ports equipped with turbo-molecular pumps. More than 99.9 % of tritium molecules is eliminated in this first differential pumping section, which is followed – in the direction pointing to pre-spectrometr – by the second differential pumping section. This one is placed in the magnetic field of 5.6 T, is operated at the temperature of 80 K and consists of tubes of 75 mm in diameter. Additional 0.04 % of tritium molecules are removed in this section.

In the next parts of transport section, both cryotrapping ones, all the remaining tritium molecules will be trapped onto the liquid helium cold surface of the transport system covered by a thin layer of argon snow and surrounded by the homogenous magnetic field ($B = 5.6$ T). The proposed diameter of the transport system tubes in this section is 75 mm.

99 % of the removed tritium molecules will be immediately returned to the inner tritium loop of the WGTS, remaining approximately 1 % molecules will be recovered by isotope separation in Tritium Labor Karlsruhe, in order to guarantee tritium purity of 95% or better.

1.4 Spectrometers

1.4.1 MAC-E-Filter

MAC-E-Filter (Magnetic Adiabatic Collimation combined with an Electrostatic Filter) is a type of spectrometers, that combine high luminosity and low background with a high resolution, both essential to measure neutrino mass from the endpoint region of a beta decay spectrum. See [1] for figures and details.

In general, MAC-E-Filter consists of two superconducting magnets placed on both sides of a cascading system of cylindrical electrodes. The beta electrons coming from the source through the entry superconducting solenoid are guided magnetically on a cyclotron motion around the magnetic field lines into the spectrometer. Then, the magnetic field drops by several orders of magnitude between the superconducting solenoid and the central plane of the spectrometer transforms most of the transversal (cyclotron) electron energy $E_\perp$ into longitudinal motion. The distance between solenoids and central analyzing plane of spectrometer is chosen in such a way, that the magnetic field B varies slowly, so the electron momentum transforms adiabatically and therefore the magnetic moment μ keeps constant

$$\mu = \frac{E_\perp}{B} = \text{const.} \tag{1}$$

So, at the central area of spectrometer, all the electrons fly almost parallel to magnetic field lines, forming a broad beam of area given by conserving magnetic field flow as

$$A_A = A_S \cdot \frac{B_S}{B_A} \tag{2}$$

with A_A being the analyzing plane area, A_S being the effective source area, B_S and B_A being magnetic fields at the source area and the analyzing plane, respectively.

This electron beam flies against the electrostatic potential formed by a system of cylindrical electrodes. Those electrons, which pass the electrostatic barrier are accelerated and guided onto a detector, the other ones are reflected. This forms an integrating high-energy pass filter.

Magnetic field at the WGTS is chosen to eliminate electrons which have a very long path within the WGTS and therefore their kinetic energy suffers from systematic uncertainity. Due to the magnetic mirror effect, the magnetic field B_S in the WGTS, the magnetic field $B_{\max}$ at the entry to the spectrometer and the maximum accepted starting angle of electrons $\vartheta_{\max}$ fulfill [5]

$$\sin \vartheta_{\max} = \sqrt{\frac{B_S}{B_{\max}}} \tag{3}$$

The final important characteristics of the MAC-E-Filter is the transmission function $R(E, T)$, i.e. the function form telling what fraction of electrons with the

initial kinetic energy E pass through the central spectrometer plane, if they are being retarded by voltage T. See [6] for detailes.

The residual transversal energy $E_\perp$ at the spectrometer analyzing plane is

$$E_\perp = E \cdot \sin^2 \vartheta \cdot \frac{B_A}{B_S} \tag{4}$$

with E being the initial kinetic energy of the electron and ϑ being the electron starting angle in the source. In order to pass through the electrostatic barrier the electron has to fulfill

$$E - E_\perp > T \tag{5}$$

i.e.

$$\sin^2 \vartheta < \frac{E-T}{E} \cdot \frac{B_S}{B_A} \tag{6}$$

Assuming isotropic beta decay and with respect to (3), the spectrometer transmission function can be written as

$$R(E,T) = \frac{1-\cos\vartheta}{1-\cos\vartheta_{\max}} \tag{7}$$

Denoting ΔE the maximal residual transversal energy (4) (the energy resolution of the spectrometer)

$$\Delta E = E \cdot \sin^2 \vartheta_{\max} \cdot \frac{B_A}{B_S} = E \cdot \frac{B_A}{B_{\max}} \tag{8}$$

the transmission function can be expressed as

$$R(E,T) = \begin{cases} 0 & E-T < 0 \\ \dfrac{1-\sqrt{1-\frac{E-T}{E}\cdot\frac{B_S}{B_A}}}{1-\sqrt{1-\frac{\Delta E}{E}\cdot\frac{B_S}{B_A}}} & 0 \le E-T \le \Delta E \\ 1 & E-T > \Delta E \end{cases} \tag{9}$$

1.4.2 MAC-E-TOF-Mode

Precise time of flight (TOF) measurement, which is feasible due to retarding electrostatic potential, can form an additional filter, effectively eliminating the low-energy electrons. Together with the high-energy electrostatic filter we acquire a non-integrating spectrometer, especially suitable for systematics study. The cost we pay is the lower count rate.

1.4.3 Pre-spectrometer

The cryotrapping sections will be followed by a MAC-E-Filter type prespectrometer, supplying the KATRIN experiment with two services

- pre-filter, rejecting all the beta electrons except the ones in the region of our interest close to the beta spectrum endpoint
- fast switch, for running the main spectrometer in the MAC-E-TOF-Mode

The prespectrometer will be a cylindrical tank 3.42 m long and 1.70 m wide in the inner diameter. The dimensions have been fixed by the electromagnetic design, especially focused on

- the magnetic fields, which should guarantee the energy resolution $\Delta E < 50\,\mathrm{eV}$, whole magnetic flux transportation and adiabacity
- eliminating local inhomogenities of the electrostatic potential
- avoiding discharges
- removing particles caught in electromagnetic traps (additional dipole electrode for active trap cleaning)

1.4.4 Main spectrometer

The KATRIN key part is the large MAC-E-Filter with the diameter of 10 m and the overall length of about 20 m, which will allow us to scan the endpoint region of the tritium beta spectrum with high luminosity and the resolution better than 1 eV. This is reached by combination of superconducting solenoids $B_{\max} = 6\,\mathrm{T}$ at the entry and the exit of the spectrometer vessel and an analyzing solenoid at the central spectrometer plane producing the magnetic field of $3 \times 10^{-4}\,\mathrm{T}$.

Electromagnetic design was done with a special care to

- removing of trapped particles, that seem to play an important role with respect to background. An additional wired electrode capable to work in both monopole and dipole regime was added to the spectrometr design to sweep the trapped particles away. The principle of removing is based on adiabiatic drift, caused by the electrostatic field perpendicular to the magnetic field.
- ideal adiabatic transport conditions. The aim is to suppress all the local magnetic and electrostatic inhomogenities violating the adiabatic energy transformation, which is crucial here.

1.5 Detector concept

The detector requirements can be summed up as follows [1, 2]:

- high efficiency for electron detection
- low gamma background

- capability to operate at high magnetic fields
- the energy resolution better than 600 eV for electron energies at the energy level of the beta spectrum endpoint
- a reasonable time resolution (better than 100 ns) for a measurement in a MAC-E-TOF-Mode
- position resolution
- possibility to absorb high count rates

The following options on detector concept were proposed

- PIN-Diode arrays. This is a standart industrial solution of pixel-detector array with single pixel sizes in the range up to $5 \times 5\,\mathrm{mm}^2$. It seems to be possible to achieve the energy resolution of 600 eV, however this resolution limit cannot be improved significantly, because of terminal capacity.
- Monolithic SDD arrays (silicon drift diodes). The SDD consist of a volume of fully depleted silicon in which an electric field with a strong component parallel to the surfaces drives the signal electrons towards a small size collecting anode with an extremely small anode capacitance. This solution offers even better energy resolution than the PIN-Diode one.
- DEPFET pixel matrices (depleted p-channel field effect transistor). This is a low noise pixel detector with the first stage amplifier integrated into the detector. It seems to be possible to achieve $\sim 10^4$ channels per cm^2 with this solution.
- Bolometers. These are thermal microcalorimeters offering the superior energy resolution of about 20–30 eV at the energy level we are interested in. The main disadvantage is the working temperature of bolometers in the mK range.

1.6 Background

The signal background is mostly dominated by:

- enviromental radioactivity and cosmic rays around the detector. This background can be suppressed by shielding and the proper choice of materials.
- tritium decays in the main spectrometers, that can be decreased under the acceptable limit by a tritium partial pressure $\simeq 10^{-20}$ mbar in the spectrometer.
- cosmic rays, especially the secondary and tertiary charged particles and ions created by cosmic rays penetration into the spectrometer and scattering inside the spectrometer. Again, a strict limit on the spectrometer vacuum can effectively suppress this contribution to background.

- trapped particles, that can be reduced by careful electrostatic and magnetic design using additional dipole electrodes inside the spectrometer.

1.7 Systematics

The main systematic errors the KATRIN experiment suffers from are:

- inelastic scattering. Note that the electron energy loss function in the tritium source (see (15) below) is dependent on 6 parameters, that are given by fit (see [7]) and make this systematic error the dominant one in the experiment.
- column density and homogenity of the tritium source. This uncertainity can be reduced by online mass spectrometry in the backward direction of the WGTS.
- $^3HeT^+$ molecule final states. An excitation energy of the first electronic excited state of the $^3HeT^+$ molecule is 27 eV. Therefore the only uncertainity comes from rotational-vibrational excitations of the daughter molecule ground state. Fortunately, both theoretical an experimental knowledge of these excitations is good.
- transmission function. The theoretical transmission function (9) we use does not include fluctuations of magnetic fields as well as electrostatic analyzing plane inhomogenities, synchrotron radiation and doppler broadening.
- trapped electrons in the WGTS and the differential pumping section. Note that we are not able to avoid local minima of the magnetic field in the WGTS and the transportation section and therefore we cannot get rid of electrons scattered on these trapped particles with slightly changed energy and momentum.
- energy scale imperfections caused by wrong calibration or time instabilities of voltmeters and a high voltage divider. This kind of systematic errors can be reduced by independent monitoring by e.g. measurening the K-32 conversion line of ^{83m}Kr.

1.8 Calibration and stability check of the energy scale

1.8.1 K-32 conversion line from gaseous ^{83}Kr

The 17.8 keV electrons are suitable for calibration and monitoring of the spectrometer energy scale [2] since their energy differs by only 0.8 keV from the endpoint

energy of the tritium beta spectrum. Concerning gaseous ^{83}Kr atoms, the electron kinetic energy E_{kin} at the detector region is

$$E_{\mathrm{kin}} = E_{\gamma} + E_{\gamma,\,\mathrm{rec}} - E_{\mathrm{b,\,vac}} - E_{\mathrm{e,\,rec}} - (\varphi_{\mathrm{spc}} - \varphi_{\mathrm{src}}) \tag{10}$$

with E_{γ} being the gamma ray energy, $E_{\gamma,\,\mathrm{rec}} = 0.0067\,\mathrm{eV}$ being the energy of a recoiled atom after a gamma ray emmision, $E_{\mathrm{b,\,vac}}$ denoting the binding energy of K shell electrons related to the vacuum level and $E_{\mathrm{e,\,rec}} = 0.120\,\mathrm{eV}$ being the energy of a recoiled atom after a conversion electron emmision. φ_{spc} and φ_{src} are work functions of the spectrometer and source chamber, respectively.

The value of $E_{\mathrm{b,\,vac}} = 14\,327.26 \pm 0.04\,\mathrm{eV}$ was determined by combination of several methods (see e.g. [8] for details), as well as the gamma ray energy of $E_{\gamma} = 32\,151.55 \pm 0.64\,\mathrm{eV}$. And finally, the value $(\varphi_{\mathrm{spc}} - \varphi_{\mathrm{src}})$ for the main KATRIN spectrometer and the WGTS can be determined by means of bunches of monoenergetic electrons of about 35 eV energy and natural widths in the meV range, which result from doubly excited ^{4}He auto-ionization states. Alternatively, the LMM Auger electrons of krypton with the energy of about 1.5 keV could be used.

1.8.2 Quench condensed $^{83\mathrm{m}}$Kr and solid ^{83}Rb sources

Concerning long time stability of the measurement, it seems not to be desirable to rely on electrical measurement only (see the next section), but to employ also a physical reference of electron energy. It could be realized e.g. by a source of K-32 electrons from ^{83}Kr, that would be connected to a third electrostatic spectrometer. Both the main and this spectrometer would be fed by a common high voltage source.

The K-32 electrons can be got from a thin ^{83}Kr film condensed on a cold backing. Since the half-life of $^{83\mathrm{m}}$Kr is 1.8 hours only a repeated condensation would be necessary. Cleaning of the backing with a laser beam and application of a pure $^{83\mathrm{m}}$Kr gas should guarantee the stability of the conversion electrons kinetic energy.

Another option on the continuous K-32 source would be a thin evaporated layer of ^{83}Rb (half-life of 86 days). See e.g. [9] for details. However using the ^{83}Rb source, it is necessary to guaratee, that

- the ^{83}Rb compounds will not escape from the backing and contaminate the spectrometer.
- the K-shell binding energy will not change during succesive change of ^{83}Rb atoms into $^{83\mathrm{m}}$Kr ones.

2 Simulation

In this section, we describe a model and algorithms we used for the KATRIN experiment simulation. Later, we are going to show that the physical predictions given by our model are in good agreement with the generally expected ones, and that the algorithms we used are accurate enough. Finally, using our routines, we are going to investigate, how the energy scale imperfections influence the KATRIN experiment sensitivity on the neutrino mass.

2.1 Integrated beta spectrum

An integrated beta spectrum as measured by MAC-E-Filter is given by the formula

$$S(T, Q, m_\nu) = \int_0^\infty \beta(E, Q, m_\nu) R'(E, T)\, \mathrm{d}E \tag{11}$$

where $\beta(E, Q, m_\nu)$ is a differential beta spectrum (12), $R'(E, T)$ denotes the spectrometer response function (14), T is the energy determined by a retarding voltage, Q stands for the maximum electron kinetic energy assuming a massless neutrino and m_ν is the neutrino rest mass.

2.1.1 Differential beta spectrum

$$\begin{aligned}\beta(E, Q, m_\nu) = N_s\, F(Z, E) \sqrt{E(E + 2m_\mathrm{e}c^2)}\left(E + m_\mathrm{e}c^2\right) \times \\ \times \sum_i \omega_i (Q - W_i - E) \sqrt{(Q - W_i - E)^2 - m_\nu^2 c^4} \times \\ \times\, \Theta(Q - W_i - E - m_\nu c^2)\end{aligned} \tag{12}$$

with N_s denoting norm of spectrum, $F(Z, E)$ being Fermi function approximation (13) (see e.g. [10] for details), Heaviside (step) function guaranteeing the energy conservation law, E denoting an electron kinetic energy, m_e being the electron rest mass, W_i standing for the i-th rotational-vibrational energy level and ω_i being the probability of a transition to this level [11]. According to [10], the Fermi function can be described as

$$F(Z, E) = \frac{x}{1 - \exp(-x)}\left(a_0 + a_1 \frac{v_\mathrm{e}}{c}\right) \qquad x = \frac{2\pi Z \alpha c}{v_\mathrm{e}} \tag{13}$$

with Z equal to 2 in our case, the fine-structure constant α, an electron velocity v_e, the speed of light in vacuum c, including the empirical values $a_0 = 1.002037$ and $a_1 = -0.001427$.

2.1.2 Response function

$$R'(E,T) = \int_0^{E-T} R(E-\varepsilon,T) \times (P_0\delta(\varepsilon) + P_1 f(\varepsilon) + P_2(f \otimes f)(\varepsilon) + \ldots)\, \mathrm{d}\varepsilon \quad (14)$$

where $R(E,T)$ is the theoretical instrumental transmission function (9) of the spectrometer, $f(\varepsilon)$ defines an electron energy loss function in gaseous tritium and P_i is the probability of an electron to be scattered i times. δ represents the Dirac δ-function and the $\otimes$ symbol denotes convolution. For details see [1].

The energy loss function is approximated [7] by

$$f(\varepsilon) = \begin{cases} A_1 \exp\left(-\frac{2(\varepsilon-\varepsilon_1)^2}{\omega_1^2}\right) & \text{for } \varepsilon < \varepsilon_c \\ A_2 \frac{\omega_2^2}{\omega_2^2 + 4(\varepsilon-\varepsilon_2)^2} & \text{for } \varepsilon \geq \varepsilon_c \end{cases} \quad (15)$$

The parameters $A_{1,2}$, $\varepsilon_{1,2}$, $\omega_{1,2}$ describe an amplitude, a mean value position and a deviation of the Gaussian and the Lorentzian, resp. The matching point ε_c is chosen in such a way that the loss function is continuous.

2.1.3 Scattering probabilities P_i

The probability of an electron going through a tritium gas to be scattered i-times is given [7] by

$$P_i' = \exp\left(-\mu\sigma_{\mathrm{tot}}\right) \frac{\left(\mu\sigma_{\mathrm{tot}}\right)^i}{i!} \quad (16)$$

with μ denoting the effective column density of tritium gas and σ_{tot} being the total inelastic cross-section. Then, the probability of an electron emitted from source in the distance x with the starting angle ϑ to be scattered i-times is proportional to

$$P_i(x,\vartheta) = \exp\left[-\frac{\sigma_{\mathrm{tot}}}{\cos\vartheta}\int_x^l \rho(y)\,\mathrm{d}y\right] \cdot \frac{\left[\frac{\sigma_{\mathrm{tot}}}{\cos\vartheta}\int_x^l \rho(y)\,\mathrm{d}y\right]^i}{i!} \quad (17)$$

where the density function of tritium gas in source $\rho(y)$ is used to parametrize the number of tritium molecules, which the electron passes and l is the source length. Note that the scattering probabilities are independent on the density function form. The relevant quantity, the probabilities are dependent on, is the number of tritium molecules, which the electron passed. In order to verify the fact, a triangle-like shape and a constant density function form were used. The obtained results were the same. The tringle-like form means

$$\rho(x) = a \cdot \begin{cases} \rho_m \cdot 10^{-2} + \frac{\rho_m(1-10^{-2})}{l/2} \cdot x & \text{for } x \in \langle 0\,;\, l/2) \\ \rho_m - \frac{\rho_m(1-10^{-2})}{l/2} \cdot (x - l/2) & \text{for } x \in \langle l/2\,;\, l\rangle \end{cases} \quad (18)$$

where a is a normalization constant, ρ_m denotes the density in the middle of the source and l is the source length. The constant density function form is then

$$\rho(x) = \frac{b}{l} \tag{19}$$

with a normalization constant b. Taking into account that the momentum direction of an electron is kept unchanged during a scattering event, the probability of electron to be scattered i-times is

$$P_i = \frac{1}{\rho_c \left(1 - \cos(\vartheta_{\max})\right)} \int_0^l \mathrm{d}x \int_0^{\vartheta_{\max}} \mathrm{d}\vartheta \ \rho(x) P_i(x, \vartheta) \sin\vartheta \tag{20}$$

where ρ_c is the tritium column density, i.e.

$$\rho_c = \int_0^l \rho(x)\,\mathrm{d}x \tag{21}$$

and the maximum accepted electron starting angle $\vartheta_{\max}$ is given by (3).

2.1.4 Normalization, constants overview

There are two independent ways, how to normalize our integrated spectra in the proper way. First, using tritium half-life, the count rate at the energy of $Q - E'$ can be written down as

$$\begin{aligned} C(Q - E') = A_A \cdot \frac{B_A}{B_S} \cdot \rho_c \cdot 2 \cdot \frac{\ln(2)}{T_{1/2}} \cdot \frac{1 - \cos(\vartheta_{\max})}{2} \cdot \varepsilon_{\mathrm{trit}} \cdot \varepsilon_{\mathrm{det}} \times \\ \times \frac{S(Q - E', Q, 0)}{\int_0^Q \beta(E, Q, 0)\,\mathrm{d}E} \end{aligned} \tag{22}$$

where A_A, ρ_c, $T_{1/2}$, $\varepsilon_{\mathrm{trit}}$, $\varepsilon_{\mathrm{det}}$ is the analyzing plane area, the tritium column density, tritium half-life, tritium purity and the detector efficiency, respectively. Also for small $m_\nu \neq 0$ the approximation is accurate enough.

Second, using the nuclear matrix element of tritium decay $\mathcal{M}$ [12], the norm of spectrum N_s can be explicitly written as

$$\begin{aligned} N_s = \frac{G_{\mathrm{F}}^2 \cos^2\Theta_{\mathrm{C}}}{2\pi^3} \left|\mathcal{M}^2\right| \left(\frac{2}{\hbar}\right)^7 \times \\ \times A_A \cdot \frac{B_A}{B_S} \cdot \rho_c \cdot 2 \cdot \frac{1 - \cos(\vartheta_{\max})}{2} \cdot \varepsilon_{\mathrm{trit}} \cdot \varepsilon_{\mathrm{det}} \end{aligned} \tag{23}$$

with G_{F} and Θ_{C} being the universal Fermi constant and Cabibbo angle, respectively.

Assuming typical values [1, 13]

$$\begin{aligned} A_A &= \pi \cdot 450^2\,\mathrm{cm}^2 \\ B_S &= 3.6\,\mathrm{T} \\ B_{\max} &= 6.0\,\mathrm{T} \\ B_A &= 3 \times 10^{-4}\,\mathrm{T} \\ \rho_c &= 5 \times 10^{17}\,\mathrm{cm}^{-2} \\ T_{1/2} &= 12.33\,\mathrm{y} \\ Q &= 18\,575\,\mathrm{eV} \\ \varepsilon_{\mathrm{trit}} &= 0.95 \\ \varepsilon_{\mathrm{det}} &= 0.9 \end{aligned} \tag{24}$$

the count rate is approximately

$$C(Q-20) \doteq 5.759\,\mathrm{s}^{-1} \tag{25}$$

Setting $\mathcal{M}$ (according to [12])

$$\left|\mathcal{M}^2\right| = 5.55\left(\frac{\hbar}{2}\right)^6 \tag{26}$$

then

$$N_s \doteq 1.76 \times 10^{-32} \times 5.04 \times 10^{18}\,\mathrm{s}^{-1}\mathrm{eV}^{-5}$$
$$N_s \doteq 8.87 \times 10^{-14}\,\mathrm{s}^{-1}\mathrm{eV}^{-5}$$

and

$$S(Q-20, Q, 0) \doteq 5.704\,\mathrm{s}^{-1} \tag{27}$$

Both values differ by factor of 1.010 and so we find them equivalent. Further on, we have decided to use the normalization method based on nuclear matrix element.

Electron energy loss function constants [7] were set as follows:

$$\begin{aligned} A_1 &= 0.204\,\mathrm{eV}^{-1} & A_2 &= 0.0556\,\mathrm{eV}^{-1} \\ \omega_1 &= 1.85\,\mathrm{eV} & \omega_2 &= 12.5\,\mathrm{eV} \\ \varepsilon_1 &= 12.6\,\mathrm{eV} & \varepsilon_2 &= 14.30\,\mathrm{eV} \end{aligned}$$

Finally, fixing

$$\begin{aligned} \sigma_{\mathrm{tot}} &= 3.456 \times 10^{-18}\,\mathrm{cm}^2 \\ \rho_m &= 10^{15}\,\mathrm{cm}^{-3} \\ l &= 10\,\mathrm{m} \end{aligned}$$

P_i values can be derived as

$$\begin{aligned} P_0 &= 0.412 \\ P_1 &= 0.293 \\ P_2 &= 0.168\ . \end{aligned}$$

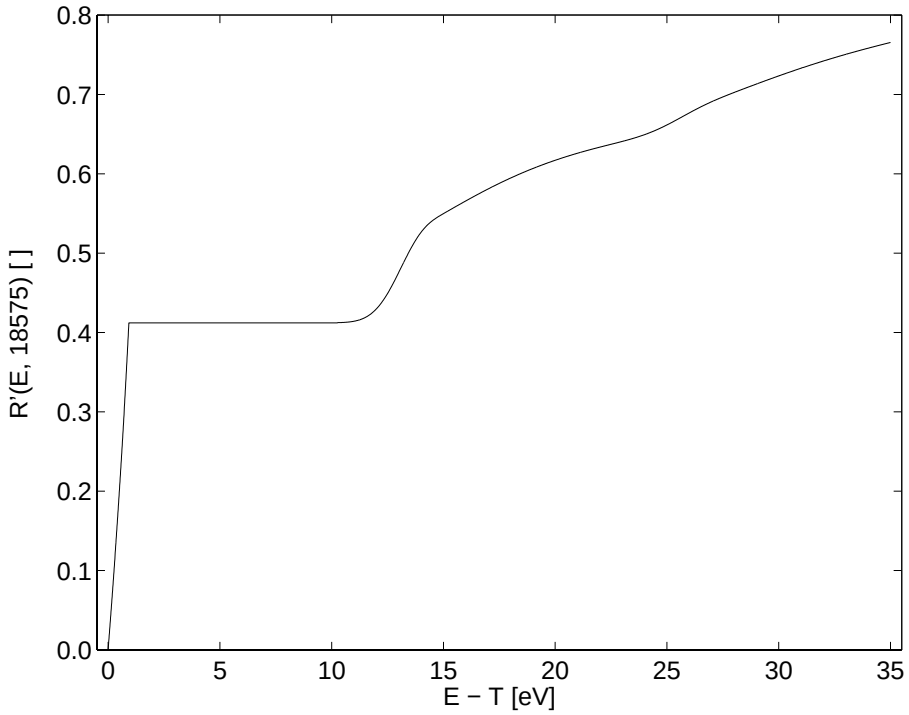

Fig. 1: Response function $R'(E, 18\,575)$

2.2 Fit

2.2.1 Least squares method

The analysis of experimental spectra is based on a minimization of the function

$$\chi^2(R_s, R_b, Q, m_\nu) = \sum_i \left(\frac{L_{\text{exp}}(T_i) - L_{\text{th}}(T_i, R_s, R_b, Q, m_\nu)}{\sigma_{\text{exp}}(T_i)} \right)^2 \tag{28}$$

by varying four free parameters, the relative norm of an electron integrated spectrum R_s, the relative norm of background R_b, the beta spectrum endpoint energy Q and the neutrino mass m_ν. $L_{\text{exp}}(T_i)$ is an experimental spectrum and $L_{\text{th}}(T_i, R_s, R_b, Q, m_\nu)$ is a theoretical spectrum.

$$L_{\text{th}}(T_i, R_s, R_b, Q, m_\nu) = R_s \cdot S(T_i, Q, m_\nu) + R_b \cdot N_b \tag{29}$$

with N_b being the amplitude of background, that was fixed equal to $N_b = 0.01\, s^{-1}$ [10] and T_i being an energy scale vector. In our simulation, the real experimental spectra are substituted by pseudoexperimental ones. It means that

$$L_{\text{exp}}(T_i) = S(T_i, Q, m_\nu) + N_b + \mathcal{N}(0,1) \cdot \sqrt{\frac{S(T_i, Q, m_\nu) + N_b}{t}}\ . \tag{30}$$

$\mathcal{N}(0,1)$ is a random number distributed normally with the mean value equal to zero and with the unit standard deviation and t stands for the total measurement time. Further,

$$\sigma_{\mathrm{exp}}(T_i) = \sqrt{\frac{S(T_i, Q, m_\nu) + N_b}{t}} \ . \tag{31}$$

Parameters $\widetilde{R}_s$, $\widetilde{R}_b$, $\widetilde{Q}$, $\widetilde{m}_\nu$ that fulfill

$$\chi^2(\widetilde{R}_s, \widetilde{R}_b, \widetilde{Q}, \widetilde{m}_\nu) = \min \chi^2(R_s, R_b, Q, m_\nu)$$

are found by a combination of simplex, Levenberg-Marquardt and Gauss-Newton method. The minimizers are searched in intervals as follows

$$\begin{aligned} R_s &\in (0.01;\, 100) \\ R_b &\in (0.01;\, 100) \\ Q &\in (18545;\, 18605) \\ m_\nu &\in (-30;\, 30) \ . \end{aligned}$$

The standard deviations of the fitted patameters are usually derived from the error matrix $\mathbf{C}$ defined as

$$\mathbf{C}^{-1}_{kl} = \sum_i \frac{\partial L_{\mathrm{th}}(T_i, \widetilde{x})}{\partial x_k} \cdot \frac{\partial L_{\mathrm{th}}(T_i, \widetilde{x})}{\partial x_l} \cdot \frac{1}{\sigma_{\mathrm{th}}(T_i, \widetilde{x})} \tag{32}$$

where $\vec{x}$ denotes the set of the fitted parameters

$$\vec{x} = \{R_s,\, R_b,\, Q,\, m_\nu\}$$

and $\widetilde{x}$ defines the set of the minimizers

$$\widetilde{x} = \{\widetilde{R}_s,\, \widetilde{R}_b,\, \widetilde{Q},\, \widetilde{m}_\nu\}$$

$\sigma_{\mathrm{th}}(T_i, \widetilde{x})$ can be expressed as

$$\sigma_{\mathrm{th}}(T_i, \widetilde{x}) = \sqrt{\frac{L_{\mathrm{th}}(\widetilde{R}_s, \widetilde{R}_b, \widetilde{Q}, \widetilde{m}_\nu)}{t}}$$

Unfortunately, this method can not be applicated in our case, because of diverging derivatives

$$\begin{aligned} \lim_{Q-E \to m_\nu +} \frac{\partial \beta(E, Q, m_\nu)}{\partial Q} &= +\infty \ , \\ \lim_{Q-E \to m_\nu +} \frac{\partial \beta(E, Q, m_\nu)}{\partial m_\nu} &= -\infty \ . \end{aligned}$$

In order to give standard deviation estimations two other methods were used. In particular, the independent measurements method and the error ellipses method [14]. None of them is based on the Taylor expansion of an integrated electron spectrum.

2.2.2 Deviation: independent measurements method

A number (1000 typically) of pseudoexperimetal spectra is created and evaluated. The derived minimizers are supposed to be a set of independent realizations of a random variable. The covariance matrix is then calculated using its definition only. The method is rough and can not be used to give a covariance matrix estimation in the case of the real experimental data. In order to describe in more detail some features of fitted parameter deviations, e.g. asymmetry, the following method was used.

2.2.3 Deviation: error ellipses method

Let us define

$$\begin{aligned} E &:= \{(R_s, R_b, Q, m_\nu) \mid \chi^2(R_s, R_b, Q, m_\nu) = \chi^2(\widetilde{R}_s, \widetilde{R}_b, \widetilde{Q}, \widetilde{m}_\nu) + 1\} \\ M &:= \{m_\nu \mid \exists R_s,\ \exists R_b,\ \exists Q,\ (R_s, R_b, Q, m_\nu) \in E\} \end{aligned} \tag{33}$$

Then the upper and the bottom estimation of the neutrino mass deviation is $\sup M - \widetilde{m}_\nu$ and $\widetilde{m}_\nu - \inf M$, respectively. The method is implemented as follows: Let $F : \mathbb{R} \longrightarrow \mathbb{R}$ be

$$F(m_\nu) = \min_{R_s, R_b, Q} \chi^2(R_s, R_b, Q, m_\nu) \tag{34}$$

where R_s, R_b, Q are free parameters, while m_ν is fixed. However the function $F(m_\nu)$ derivatives tend to vanish locally, so two different methods are used to find out $\sup M$ and $\inf M$ values. In the first case, $\sup M$, $\inf M$ is obtained as m'_ν fulfilling

$$\left|F(m'_\nu) - \chi^2(\widetilde{R}_s, \widetilde{R}_b, \widetilde{Q}, \widetilde{m}_\nu) - 1\right| = \min \left|F(m_\nu) - \chi^2(\widetilde{R}_s, \widetilde{R}_b, \widetilde{Q}, \widetilde{m}_\nu) - 1\right| \tag{35}$$

in the region $(-\infty,\ \widetilde{m}_\nu)$, $(\widetilde{m}_\nu,\ \infty)$, respectively. In the second case, $\sup M$, $\inf M$ is found as m'_ν solving

$$F(m'_\nu) - \chi^2(\widetilde{R}_s, \widetilde{R}_b, \widetilde{Q}, \widetilde{m}_\nu) - 1 = 0 \tag{36}$$

in the region $(-\infty,\ \widetilde{m}_\nu)$, $(\widetilde{m}_\nu,\ \infty)$, respectively. The error ellipses method can be used to analyze each specific case separately, as well as it can be applied to unrandomized spectra, in order to study systematics. However the method, as implemented, provides no information about correlation coeficients of the fitted parameters. The method respects a possible asymmetry of χ^2. We consider this fact to be the main advantage of the error ellipses method.

2.3 Negative neutrino mass

Let us try to investigate the electron spectra with the vanishing neutrino mass by the independent measurements method. Due to normal randomization of spectra, a half fits should fall in a negative neutrino mass region. Later, we are going to show that the real experimental spectra could suffer with systematic errors that generate a fictitious neutrino mass (both positive and negative). In order to study this kind of systematics as well as to do proper simulation in the previous case, we need a way how to deal with the fictive negative neutrino mass.

We would like to emphasize that we are not looking for a negative mass beta spectrum, because *it does not exist.* Also a negative mass neutrino should be strictly considered not to be physical. We are seeking a function form $\beta'(E, Q, m_\nu)$. Note that there is no way the parameters Q and m_ν would be connected to the total decay energy and the neutrino mass. Let us define

$$\beta(E, Q, m_\nu) = \begin{cases} \text{equation (12)} & \text{for } m_\nu \geq 0 \\ \beta'(E, Q, m_\nu) & \text{for } m_\nu < 0 \end{cases}$$

We request the new $\beta(E, Q, m_\nu)$ function to fulfill the following requirements:

1. *symmetric* χ^2

Let $\chi_1^2(R_s, R_b, Q, m_\nu)$ be the χ^2 function (28) for

$$L_{\text{exp}}(T_i) = L_{\text{th}}(T_i, R'_s, R'_b, Q', m'_\nu)$$

So the set $\{R'_s, R'_b, Q', m'_\nu\}$ minimizes χ_1^2. Let $\chi_2^2(R_s, R_b, Q, m_\nu)$ be the χ^2 function for

$$L_{\text{exp}}(T_i) = L_{\text{th}}(T_i, R'_s, R'_b, Q', -m'_\nu)$$

The set of χ_2^2 minimizers is $\{R'_s, R'_b, Q', -m'_\nu\}$. Then we request

$$\chi_1^2(R'_s, R'_b, Q', m_\nu) = \chi_2^2(R'_s, R'_b, Q', -m_\nu) \tag{37}$$

Note that χ^2 is not required to be parabolic, neither in a zero neutrino mass region, nor anywhere else. The reason is the fact that S function is not linear in m_ν.

2. *as smooth as possible*

The new β function should be at least continuous as a function of m_ν.

2.3.1 Our approach

Restricting $m_\nu \geq 0$, the function $\beta(E, Q, m_\nu)$ of equation (12), has been derived using the four-fermion interaction quantum field model and the static approximation (the recoil energy omitted, all members of order "total decay energy / [tritium mass + helium mass]" or higher neglected). Omitting the daughter molecule

rotational-vibrational states, the only member in the formula (12) connected to the neutrino mass is

$$(Q-E)\sqrt{(Q-E)^2-m_\nu^2c^4} \tag{38}$$

Indeed the expression (38) comes from $E_\nu p_\nu$ (if the total decay energy is fixed to $Q+m_\mathrm{e}$) where E_ν is the neutrino total energy and p_ν denotes the neutrino momentum. Expanding the expression (38) into Taylor series assuming $m_\nu^2c^4 < (Q-E)^2$ we get

$$(Q-E)^2\left[1-\frac{\xi^2}{2}-\frac{\xi^4}{8}-\frac{\xi^6}{16}-\frac{5\xi^8}{128}-\frac{7\xi^{10}}{256}+\ldots\right] \tag{39}$$

with ξ denoting

$$\xi := \left(\frac{m_\nu c^2}{Q-E}\right)^2$$

In the case of the vanishing neutrino mass the expression (38) becomes $(Q-E)^2$. As for the negative m_ν parameter we find natural to substitute (39) for

$$(Q-E)^2\left[1+\frac{\xi^2}{2}+\frac{\xi^4}{8}+\frac{\xi^6}{16}+\frac{5\xi^8}{128}+\frac{7\xi^{10}}{256}+\ldots\right] \tag{40}$$

However, this form can not be used, because it is divergent in a region $E \longrightarrow Q$. We can accept ξ^2, but not ξ to higher order. We can either restrict the series up to two members or look for a similar nondivergent series. The first possibility does not seem to be precise enough. Regarding the other one, we have finally picked up the series

$$(Q-E)^2\left[1+\frac{\xi^2}{2}-\frac{\xi^4}{8}+\frac{\xi^6}{16}-\frac{5\xi^8}{128}+\frac{7\xi^{10}}{256}+\ldots\right] \tag{41}$$

that can be summed up to

$$(Q-E)\sqrt{(Q-E)^2+m_\nu^2c^4} \tag{42}$$

So the function $\beta'(E,Q,m_\nu)$ form is chosen to be (see fig. 2)

$$\begin{aligned}\beta'(E,Q,m_\nu) = {} & N_s\,F(Z,E)\sqrt{E(E+2m_\mathrm{e}c^2)}\left(E+m_\mathrm{e}c^2\right)\times \\ & \times\sum_i \omega_i(Q-W_i-E)\sqrt{(Q-W_i-E)^2+m_\nu^2c^4}\times \\ & \times\Theta(Q-W_i-E)\end{aligned} \tag{43}$$

2.3.2 Negative neutrino mass squared

We are going to show later (see section 3.4.3) that the neutrino mass is not the correct physical parameter to be fitted. The neutrino mass squared is the proper one. In order to incorporate the neutrino mass squared into our calculations, it is neccessary to rearrange our fitting procedure (see section 3.2) in the way, that the

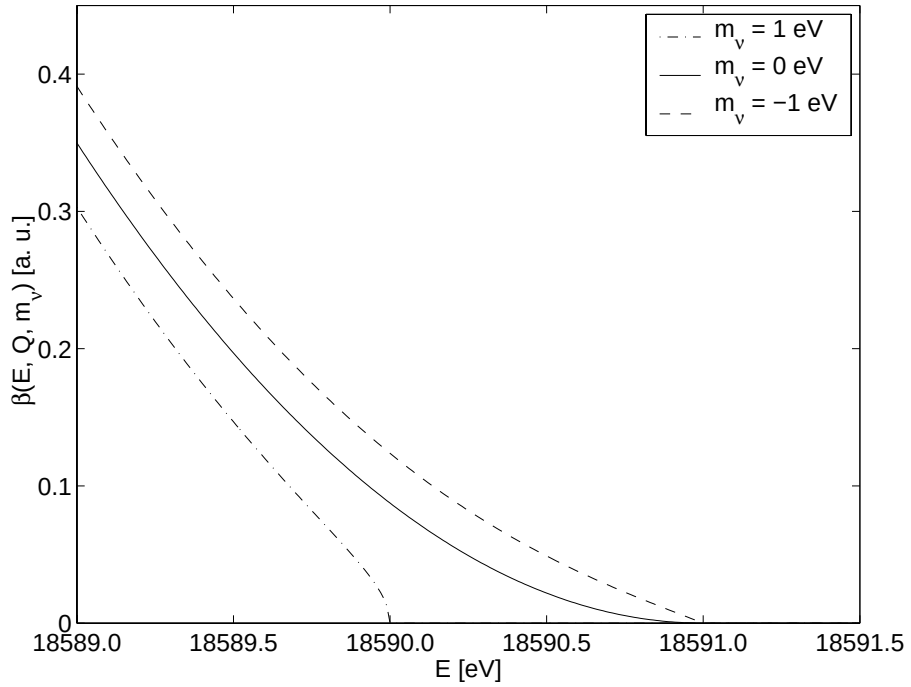

Fig. 2: Differential beta spectrum $\beta(E, 18591, m_\nu)$, ro-vi states neglected

neutrino mass is replaced by the neutrino mass squared, except for the integrated beta spectrum S, which is evaluated in $S(T, Q, \sqrt{m_\nu^2})$ instead of $S(T, Q, m_\nu)$. From this point of view, it seems to be natural not to prolong the beta spectrum formula into the negative mass region, but into the negative mass squared one. Following the ideas of the previous section, this can be easily done. The result for $m_\nu^2 < 0$ is

$$\begin{aligned}\beta'(E, Q, m_\nu^2) = {} & N_s\, F(Z, E) \sqrt{E(E + 2m_\mathrm{e}c^2)}\, \left(E + m_\mathrm{e}c^2\right) \times \\ & \times \sum_i \omega_i (Q - W_i - E) \sqrt{(Q - W_i - E)^2 - m_\nu^2 c^4} \times \\ & \times \Theta(Q - W_i - E)\end{aligned} \tag{44}$$

Fig. 3 shows χ^2 form (28) for both linear and squared neutrino mass.

2.3.3 Further improvement

In our point of view, the accuracy of the formula (43) seems to be sufficient, but further improvement is possible. For example, in the region fulfilling the condition $m_\nu^2 c^4 \ll (Q - E)^2$ more precise formula (40) could be used, in the energy region very nearby to Q we could restrict the Taylor expansion up to the order of ξ^2 and the region in between could be overcome by any suitable smooth function form.

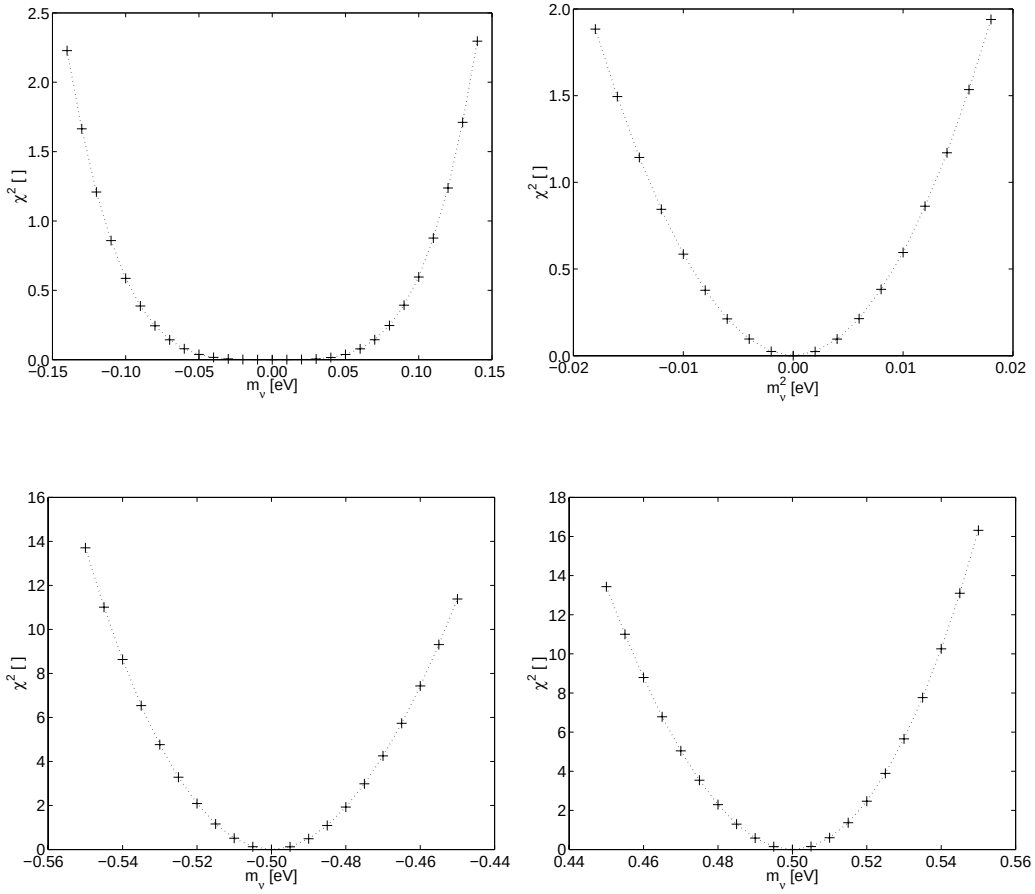

Fig. 3: $\chi^2(R'_s, R'_b, Q', m^2_\nu)$ function plot (upper right picture) and $\chi^2(R'_s, R'_b, Q', m_\nu)$ function plots (the other pictures) (see (28)); $L_{\mathrm{exp}}(T_i) = L_{\mathrm{th}}(T_i, R'_s, R'_b, Q', m^{2\prime}_\nu)$ (upper right one), $L_{\mathrm{exp}}(T_i) = L_{\mathrm{th}}(T_i, R'_s, R'_b, Q', m'_\nu)$ (the other ones), $T_i \in \{18\,545.0,\ 18\,545.5,\ 18\,546.0,\ ...,\ 18\,577.0\}$. The parameters used for the pseudoexperimental spectrum creation were: $R'_s = 1$, $R'_b = 1$, $Q' = 18\,575\,\mathrm{eV}$, $m^{2\prime}_\nu$ being $0.0\,\mathrm{eV}$ and m'_ν being $0.0\,\mathrm{eV}$ in the upper left picture, $-0.5\,\mathrm{eV}$ in the bottom left one and $0.5\,\mathrm{eV}$ in the bottom right picture. The "measurement" time was one year, time spent in each point of spectrum was equal

2.4 Neutrino mass variance properties

2.4.1 Numerical precision

All simulation were done using MATLAB programming system. In order to guarantee, that our program works in correct way, theoretical unrandomized spectra were evaluated for a broad region of input parameters. Differencies between the initial (creating) and the final (fitted) neutrino mass were observed. The worst value was less than $10^{-5}\,\mathrm{eV}$, typical value was less than $10^{-7}\,\mathrm{eV}$; restricting us to the massless neutrino, typical values were below $10^{-8}\,\mathrm{eV}$.

2.4.2 Linear or squared mass

Based on the knowledge of the neutrino mass deviation, the neutrino mass squared deviation can be derived as follows

$$\sigma^{\pm}_{m^2_\nu} = 2m_\nu \sigma^{\pm}_{m_\nu} \pm \left(\sigma^{\pm}_{m_\nu}\right)^2 \tag{45}$$

with σ^+ and σ^- denoting the upper and the lower bound of the deviation. It means, that the results can be presented in the following manner

$$\overline{x}\ {}^{+\sigma^+}_{-\sigma^-} \tag{46}$$

with $\overline{x}$ being the mean value of the appropriate physical quantity.

In order to compare mass squared deviation obtained by fitting the linear mass and the mass squared, we should distinguish the physical results and the other ones. If our fit is not influenced by the nonphysical part of the differential beta spectrum (see (43) and (44)) then the result can be treated as the physical one. Tab. 1 and tab. 2 show the physical results comparison. Pseudoexperimental unrandomized spectra from $18\,545\,\mathrm{eV}$ to $18\,577\,\mathrm{eV}$ with $0.5\,\mathrm{eV}$ step were evaluated by the error ellipses method. The total measurement time was set to one year, and the particular time spent in each point of spectra was the same.

So all the physical predictions we can make do not depend on whether we fit the linear neutrino mass or the mass squared. Regarding the other cases, equation (45) is not fulfilled, because in general we are not able to reconstruct negative square mass values by squaring results, that were obtained by linear neutrino mass fits.

Further on, we have decided to evaluate spectra using the neutrino linear mass, because nobody had ever tried to do it and because the neutrino mass is what we are interested in.

m_ν [eV]	$\sigma^+_{m_\nu}$ [eV]	$\sigma^+_{m^2_\nu}$ der. [eV^2]	$\sigma^+_{m^2_\nu}$ fit. [eV^2]	δ [eV^2]
0.00	0.205 973 6	0.042 425 1	0.042 425 1	$< 10^{-7}$
0.05	0.161 984 7	0.042 437 5	0.042 437 5	$< 10^{-7}$
0.10	0.129 050 5	0.042 464 1	0.042 464 1	$< 10^{-7}$
0.15	0.104 946 1	0.042 497 5	0.042 497 5	$< 10^{-7}$
0.20	0.087 320 1	0.042 552 8	0.042 552 8	$< 10^{-7}$
0.25	0.074 235 2	0.042 628 5	0.042 628 5	$< 10^{-7}$
0.30	0.064 318 5	0.042 728 0	0.042 728 0	$< 10^{-7}$
0.35	0.056 616 2	0.042 836 7	0.042 836 7	$< 10^{-7}$
0.40	0.050 503 0	0.042 952 9	0.042 952 9	$< 10^{-7}$
0.45	0.045 577 8	0.043 097 4	0.043 097 4	$< 10^{-7}$
0.50	0.041 525 8	0.043 250 2	0.043 250 2	$< 10^{-7}$

Tab. 1: Comparison of the physical predictions on the upper neutrino mass squared deviation. $\sigma^+_{m_\nu}$ column shows results obtained by linear neutrino mass fits. The third column gives eq. (45) solutions, the fourth one is obtained by neutrino mass squared fits. The last column shows differencies δ between derived and fitted mass squared deviations. See text for spectra parameters

m_ν [eV]	$\sigma^-_{m_\nu}$ [eV]	$\sigma^-_{m^2_\nu}$ der. [eV^2]	$\sigma^-_{m^2_\nu}$ fit. [eV^2]	δ [eV^2]
0.40	0.057 595 0	0.042 758 8	0.042 758 8	$< 10^{-7}$
0.45	0.050 495 1	0.042 895 8	0.042 895 8	$< 10^{-7}$
0.50	0.045 090 4	0.043 057 2	0.043 057 2	$< 10^{-7}$
0.55	0.040 798 8	0.043 214 1	0.043 214 1	$< 10^{-7}$
0.60	0.037 327 9	0.043 400 1	0.043 400 1	$< 10^{-7}$

Tab. 2: Comparison of the physical predictions on the lower estimate of the neutrino mass squared deviation. $\sigma^-_{m_\nu}$ column shows results obtained by linear neutrino mass fits. The third column gives eq. (45) solutions, the fourth one is obtained by mass squared fit. The last column shows differencies δ between derived and fitted mass squared deviations. See text for spectra parameters

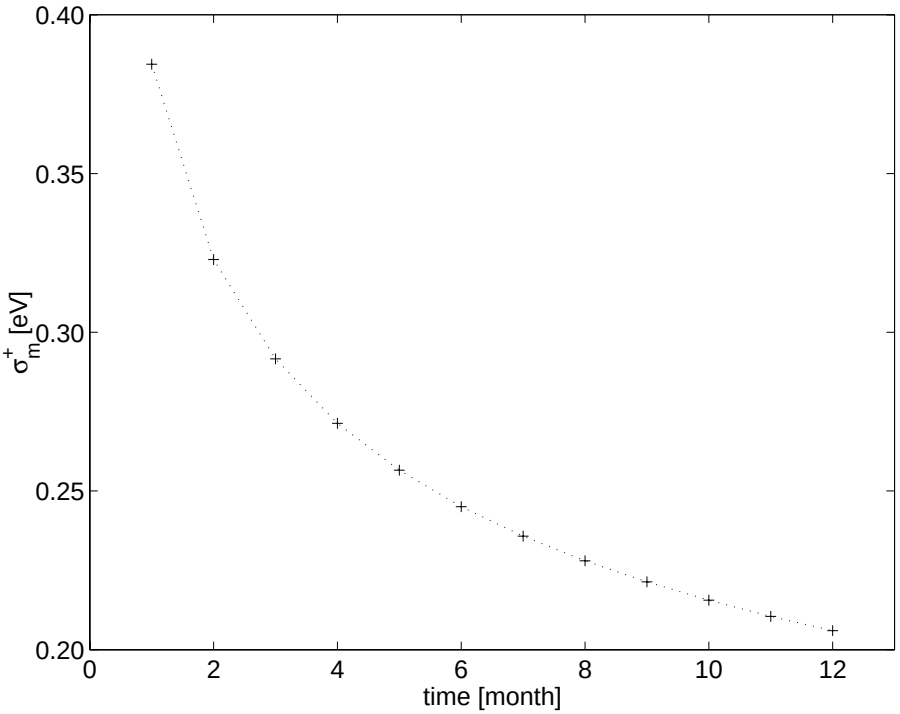

Fig. 4: Dependence on the measurement time of the upper estimation on the neutrino mass deviation. See text for spectra parameters

2.4.3 Dependence on the total measurement time

Pseudoexperimental spectra ($L_{\mathrm{exp}}(T_i) = L_{\mathrm{th}}(T_i, 1.0, 1.0, Q, m_\nu)$, see (29)) from 18 545 eV to 18 577 eV with 0.5 eV step were evaluated by the error ellipses method. An equal time was spent in each point of the spectrum. The neutrino was assumed to be massless. The background amplitude was considered to be 10 mHz. The obtained results are shown in fig. 4 and fig. 5.

In general, reciprocal dependence of a fitted physical parameter variance on the measurement time is expected. Fig. 6 demonstrates with resonable precision, that the neutrino mass deviation approximately fulfills (assuming the vanishing neutrino mass)

$$\frac{t}{t'} = \left(\frac{\sigma'_m}{\sigma_m}\right)^4 = \left(\frac{\sigma'_{m^2}}{\sigma_{m^2}}\right)^2 \tag{47}$$

We can conclude, that the neutrino mass squared is the correct physical parameter in our experiment.

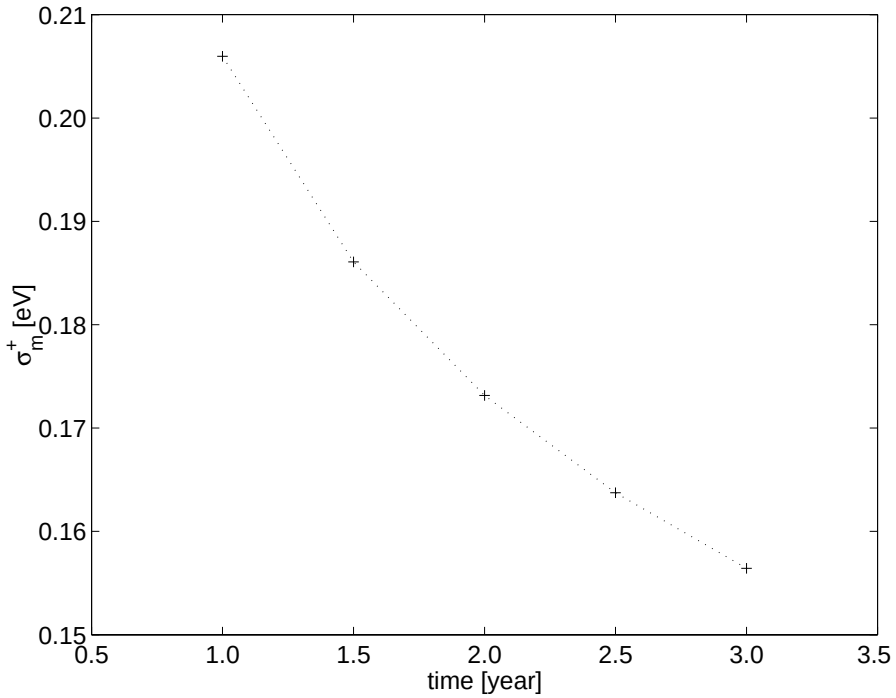

Fig. 5: Dependence on the measurement time of the upper estimation on the neutrino mass deviation. See text for spectra parameters

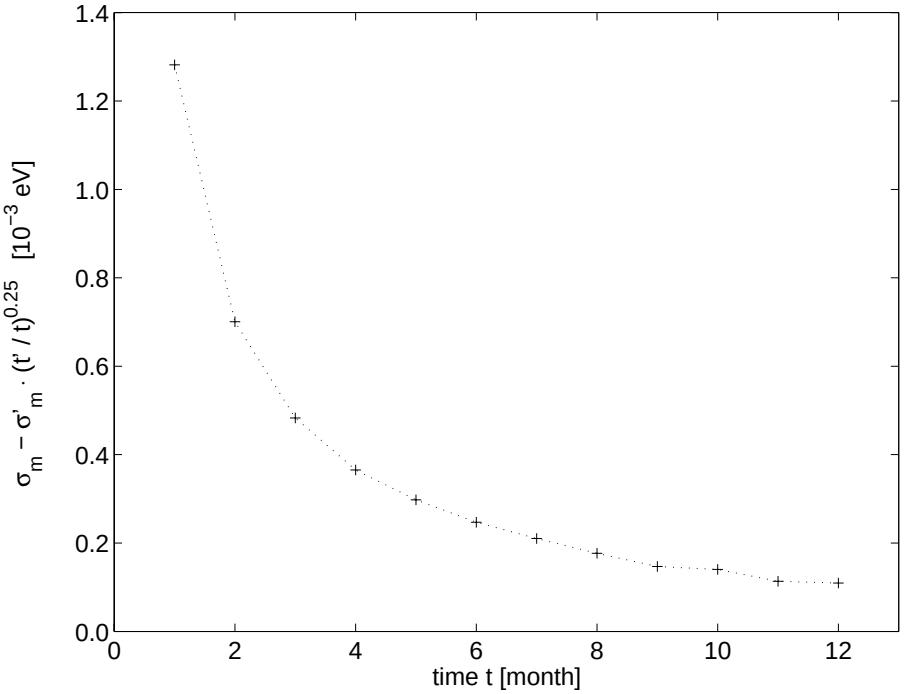

Fig. 6: Differencies between the simulated neutrino mass deviation and the expected value according to (47). t' was chosen equal to 3 years

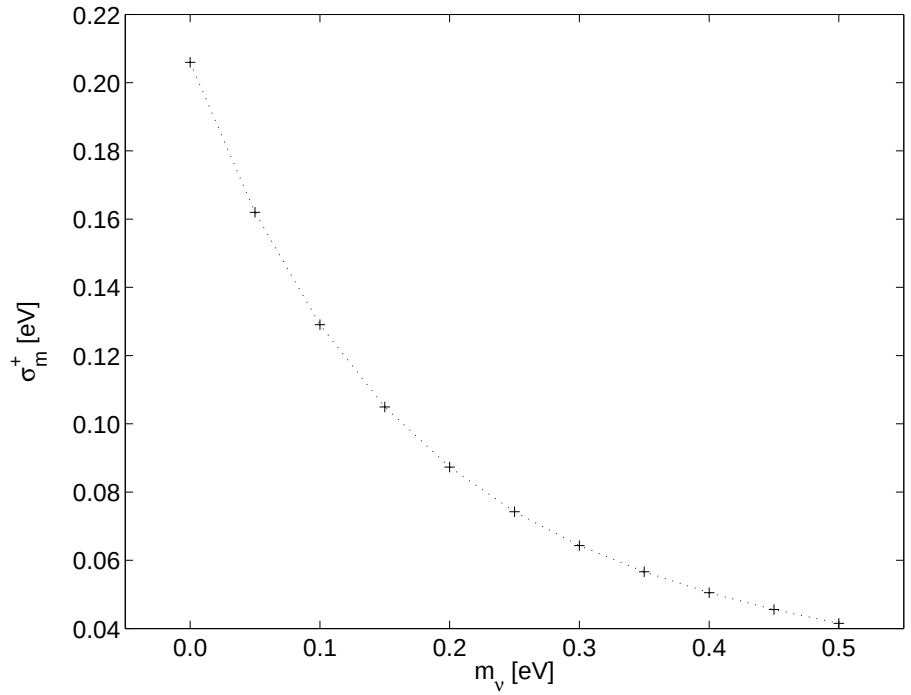

Fig. 7: Dependence of the neutrino mass deviation on the neutrino mass. The spectra from 18 545 eV to 18 577 eV with 0.5 eV step were "measured" for 1 year

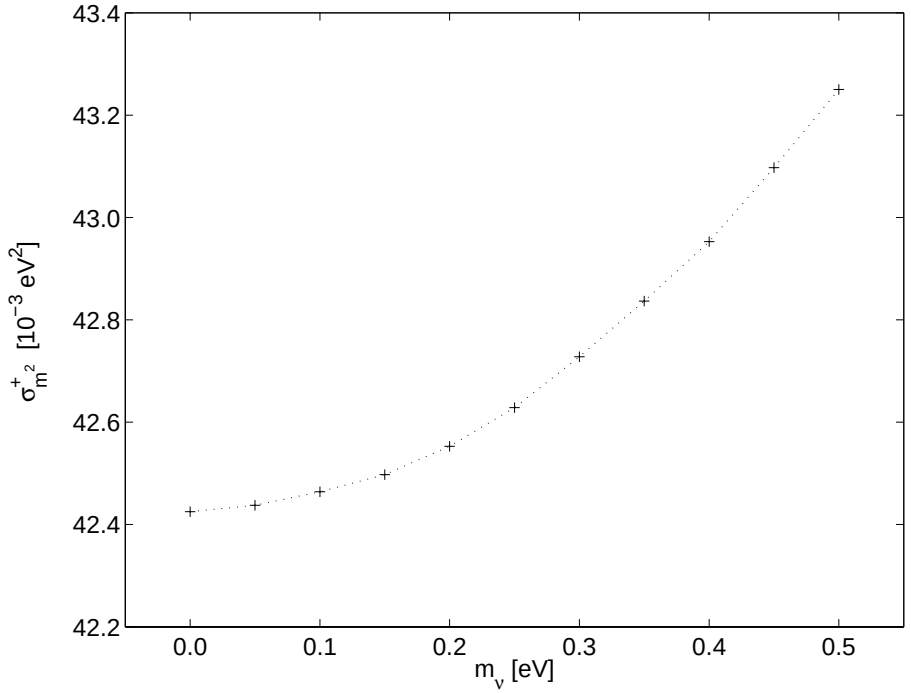

Fig. 8: Dependence of the neutrino mass squared deviation on the neutrino mass. Spectra parameters were the same as those in fig. 7

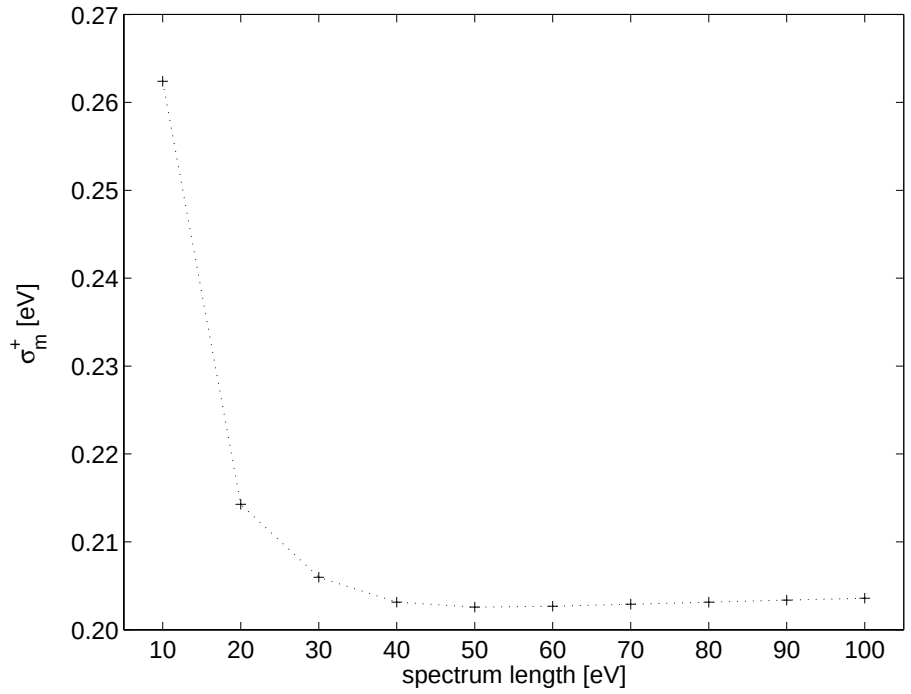

Fig. 9: Dependence of the neutrino mass deviation on the spectrum length. The x-scale values are the distances from the beginnings of spectra to the beta spectrum endpoint Q. See text for details on spectra parameters

2.4.4 Dependence on the neutrino mass

The error ellipses method was used to examine how the neutrino mass deviation is influenced by the neutrino mass itself. Unrandomized spectra were measured in the same points as in the previous case. One year measurements and 10 mHz constant background noise are assumed. The result is shown in fig. 7 and fig 8.

With good accuracy, the deviation of the neutrino mass squared is constant and independent on the neutrino mass.

2.4.5 Dependence on the spectrum length

Dependence of the neutrino mass deviation on the spectrum length was studied by the error ellipses method. A measurement lasting for one year was assumed. The final point of the spectrum was chosen to be $Q + 2\,\mathrm{eV}$ and the spectrum step was 0.5 eV. Simulations for the spectrum beginnings in the region from $Q - 10\,\mathrm{eV}$ to $Q - 100\,\mathrm{eV}$ and the vanishing neutrino mass were done. Fig. 9 shows the result.

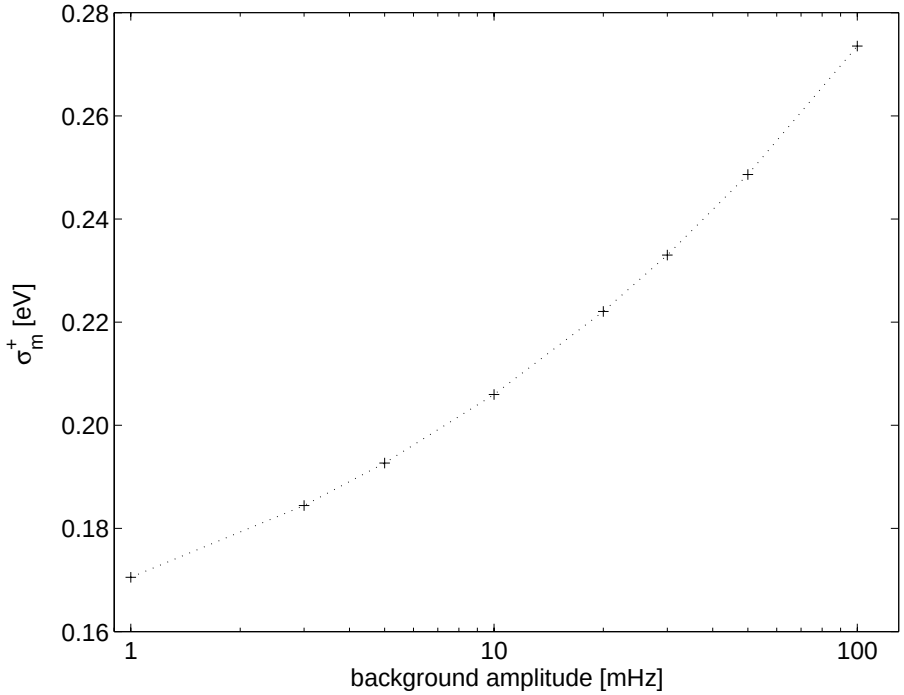

Fig. 10: Dependence of the neutrino mass deviation on the background amplitude. See text for the spectra parameters

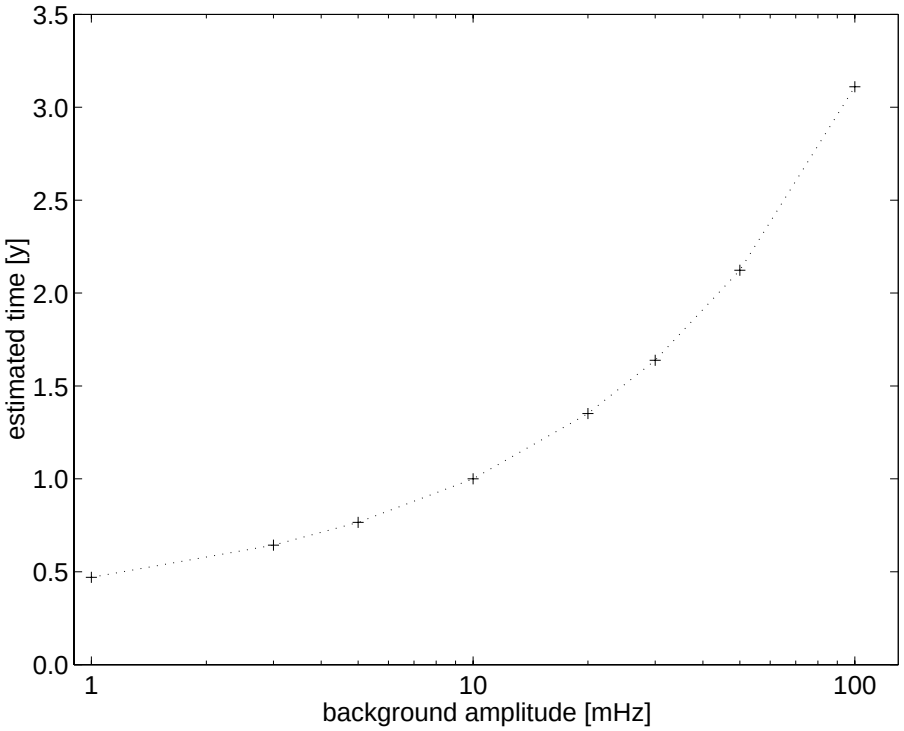

Fig. 11: The total measurement time dependence on background amplitude. The plot shows the estimation of the measurement time needed to reach the same sensitivity on the neutrino mass as one year measurement with 10 mHz background

2.4.6 Dependence on the background amplitude

Pseudoexperimental spectra from 18 545 eV to 18 577 eV with 0.5 eV step were evaluated by the error ellipses method. The time spent in each point of the spectrum was equal. Neutrino was considered to be massless. The total measurement time was set to one year. Fig. 10 illustrates the dependence of the neutrino mass deviation on the background amplitude.

The question, how long measurement is neccessary in order to achieve the same sensitivity on the masless neutrino for different background amplitudes is answered in fig. 11. One year measurement with 10 mHz background was picked up as our reference spectrum.

2.4.7 The covariance matrix

The diagonal elements of the matrix below give deviations and the offdiagonal ones show the correlation coefficients. The matrix was derived by the independent measurements method assuming 2 500 one year spectra in the energy bins from 18 545 eV to 18 577 eV with 0.5 eV step. The initial neutrino mass was $m_\nu = 0$ eV and the background amplitude was 10 mHz. The fit was done using the linear neutrino mass in the first case and the mass squared in the second one.

$$\begin{array}{c} \\ R_s \\ R_b \\ Q \\ m_\nu \end{array} \begin{array}{c} \begin{array}{cccc} R_s & R_b & Q & m_\nu \end{array} \\ \begin{pmatrix} 4.602 \times 10^{-4} & -0.211 & -0.968 & -0.759 \\ . & 4.481 \times 10^{-3} & 0.281 & 0.420 \\ . & . & 4.144 \times 10^{-3} & 0.861 \\ . & . & . & 1.896 \times 10^{-1} \end{pmatrix} \end{array}$$

Fit $\chi^2 = 60.75$. Note that there are 61 degrees of freedom.

$$\begin{array}{c} \\ R_s \\ R_b \\ Q \\ m_\nu^2 \end{array} \begin{array}{c} \begin{array}{cccc} R_s & R_b & Q & m_\nu^2 \end{array} \\ \begin{pmatrix} 4.467 \times 10^{-4} & -0.198 & -0.967 & -0.783 \\ . & 4.390 \times 10^{-3} & 0.272 & 0.422 \\ . & . & 4.023 \times 10^{-3} & 0.894 \\ . & . & . & 4.418 \times 10^{-2} \end{pmatrix} \end{array}$$

Fit $\chi^2 = 61.14$.

Note that the deviation of the relative spectrum amplitude, the relative background amplitude and the beta spectrum endpoint, as well as all the correlation coefficients are independent on the manner the neutrino mass is fitted (whether as the linear neutrino mass or the mass squared).

2.4.8 Confidence levels

In order to connect our physical predictions on the neutrino mass deviation with a confidence level, knowledge of the neutrino mass cumulative distribution function is needed. This can be estimated by integrating the neutrino mass histogram. So, 2 500 spectra were evaluated assuming the vanishing neutrino mass. Histograms of all the fitted parameters as well as of minima of χ^2 (28) are shown in Fig. 12 (the linear neutrino mass was fitted) and Fig. 13 (the mass squared was fitted). Note that the histograms are valid for the given parameters only.

Trying to explain the strange function form of the neutrino mass density, the following argument can be used: Let $H(m_\nu^2)$ be the neutrino mass squared density function. Then, the neutrino mass density function $G(m_\nu)$ can be approximated as

$$G(m_\nu) = H(m_\nu^2) \cdot |2m_\nu| \ . \tag{48}$$

Focusing on the zero neutrino mass region, it is obvious now, that any finite mass squared density function implies vanishing linear mass density function.

Integrating the neutrino mass density function, assuming that the negative neutrino mass region is unphysical and using Bayesian approach the following forecast can be given: Let us measure the integrated beta spectrum in the points from 18 545 eV to 18 577 eV with 0.5 eV step for 1 year. Further, let the least square fit result be $m_\nu = 0\,\mathrm{eV}$. The upper bound of neutrino mass deviation estimated by the error ellipses method fitting the linear mass is $\sigma^+_{\mathrm{m}_\nu} = 0.206\,\mathrm{eV}$. Then we can conclude that the upper bound for a massless neutrino is approximately 0.206 eV on 65.8 % c. l. and 0.267 eV on 90 % c. l. The 65.8 % c. l., given by neutrino mass deviation, and 90 % c. l. are connected approximately by the factor of 1.29.

As for the neutrino mass squared predictions obtained by the neutrino mass squared fitting, the following statment can be done, with respect to the neutrino mass squared deviation value $0.0424\,\mathrm{eV}^2$ derived by the error ellipses method. The sensitivity upper bound of the vanishing neutrino mass squared is $0.0424\,\mathrm{eV}^2$ on 66.4 % c. l., that is $0.0690\,\mathrm{eV}^2$ on 90 % c. l., resulting in 1.64 multiplicative factor between the mass squared deviation and 90 % c. l.

Regarding a 3 year measurement and assuming the same multiplicative factors, the massless neutrino upper bounds are 0.203 eV on 90 % c. l. (fitting the linear neutrino mass) and $0.0398\,\mathrm{eV}^2$ on 90 % c. l. (the fitting mass squared).

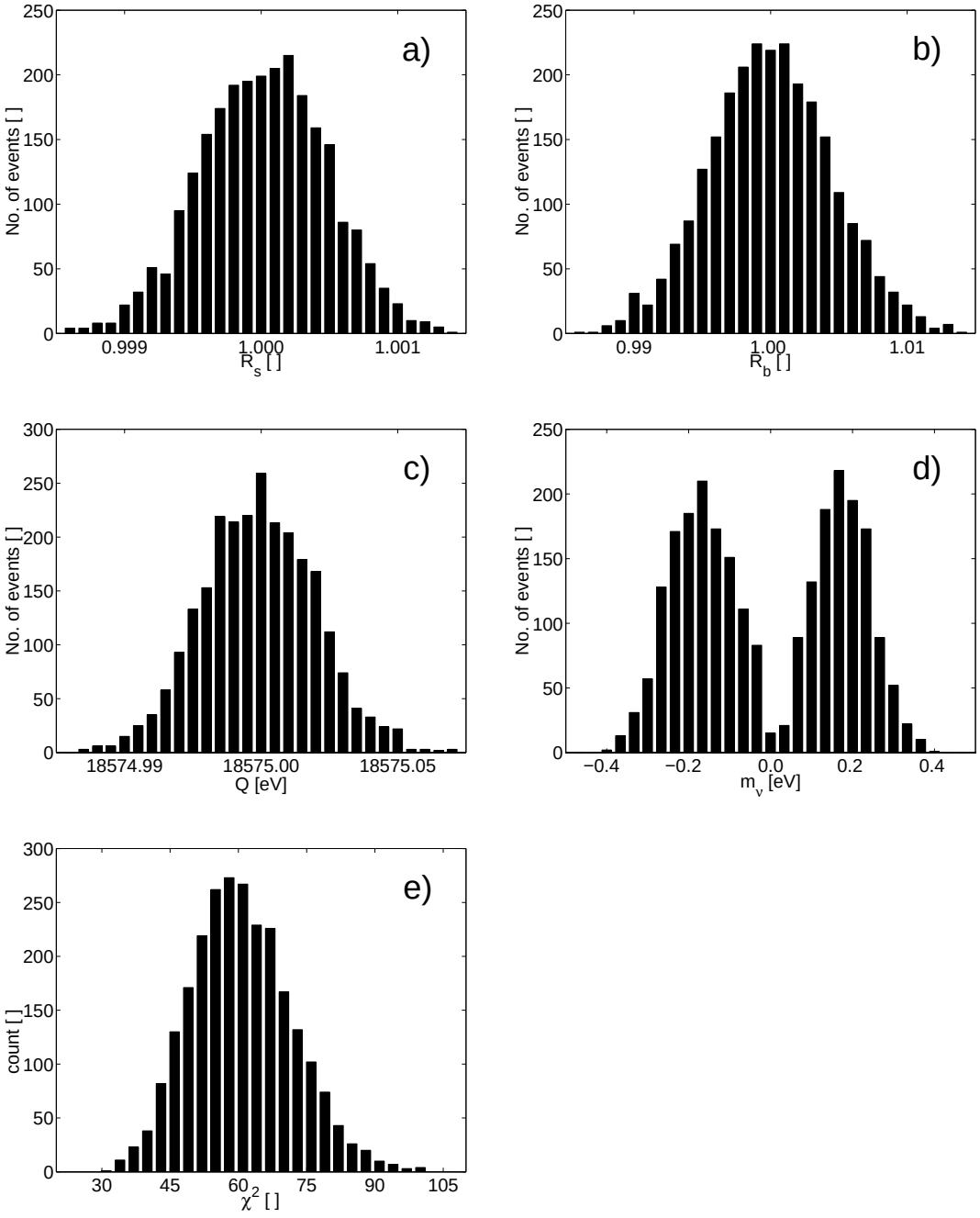

Fig. 12: Relative spectrum amplitude (a), relative background amplitude (b), the beta spectrum endpoint (c), the neutrino mass (d) and χ^2 (e) histograms obtained by 2 500 spectra evaluating by the independent measurements method. The linear neutrino mass was fitted. Spectra from 18 545 eV to 18 577 eV with 0.5 eV step were created assuming vanishing neutrino mass, one year measurement and 10 mHz background amplitude

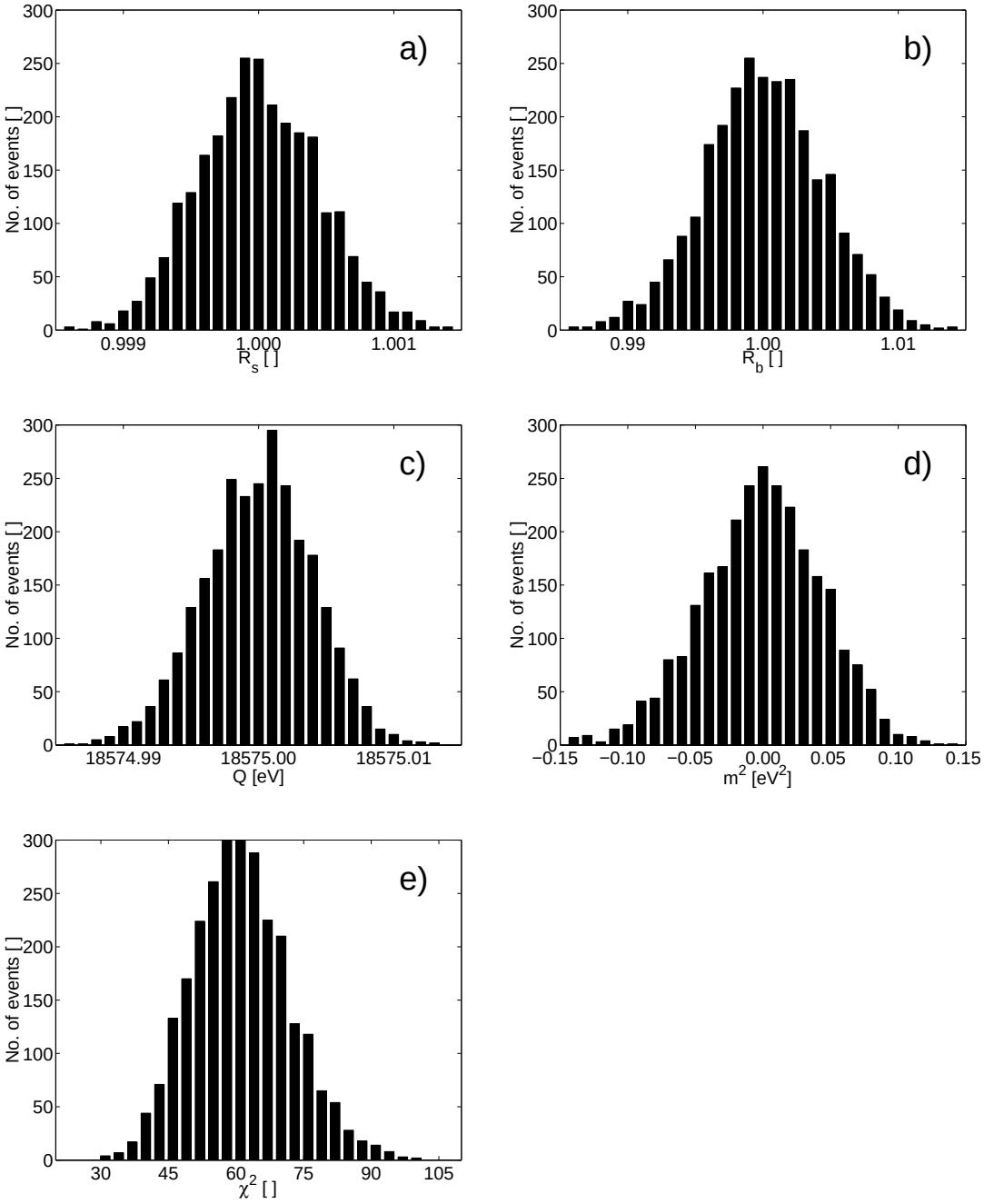

Fig. 13: Relative spectrum amplitude (a), relative background amplitude (b), the beta spectrum endpoint (c), the neutrino mass squared (d) and χ^2 (e) histograms, obtained by 2 500 spectra evaluating by the independent measurements method. The neutrino mass squared was fitted. Spectra from 18 545 eV to 18 577 eV with 0.5 eV step were created assuming vanishing neutrino mass, one year measurement and 10 mHz background amplitude

2.4.9 Dependence on the resolution

The neutrino mass dependece on the energy resolution was examined as well. Spectra from 18 545 eV to 18 577 eV with 0.5 eV step were evaluated by the error ellipses method. The time spent in each point of spectra was equal. The results are shown in Fig. 14

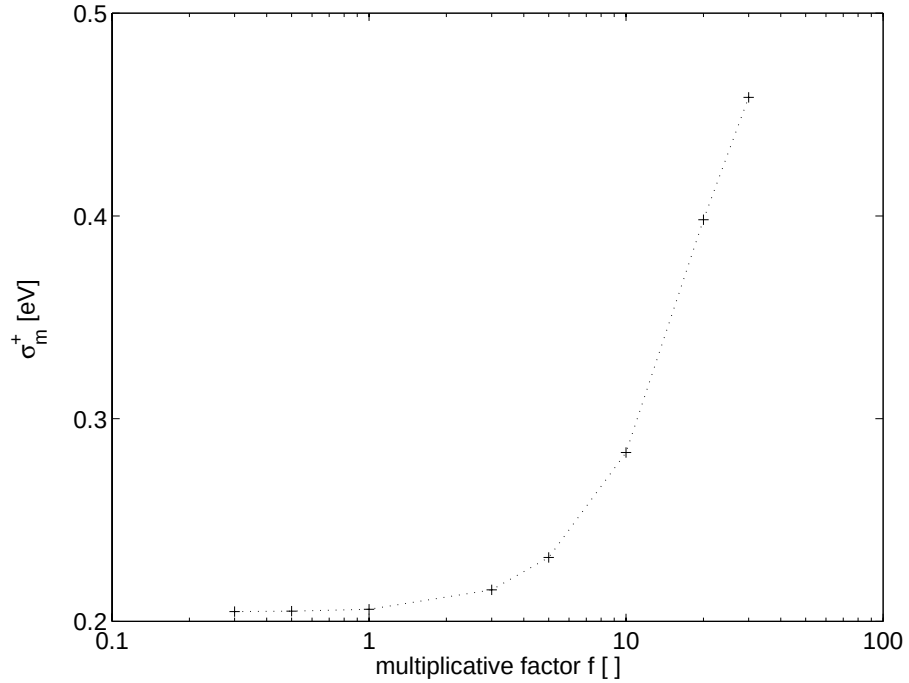

Fig. 14: Dependence of the neutrino mass deviation on the resolution at the beta spectrum endpoint. The spectra were evaluated using the analyzing magnetic field $B_A \cdot f$ and the analyzing plane area A_A/f. Note that the resolution is proportional to the magnetic field (8). For spectra parameters see text

2.5 Energy scale imperfections

There exist several kinds of energy scale imperfections. We are not going to study them all. Instead, we would like to investigate the typical ones. We have picked up two of them: wrong calibration and time instabilities.

Note that we are not interested in instabilities of high voltage sources, DAC/ADC imperfections etc., because both count rate and voltage are stored during our measurement. So the failures of a voltmeter and a high voltage divider are the only things we are taking into account. These can manifest themself typically as: an energy scale bias and an improper slope of the calibration line.

2.5.1 Constant energy bias

Let us assume, that a wrong calibration of our volmeter leads to a bias of the energy scale and that the bias is kept unchanged during the measurement. The question is, whether and how the fitted neutrino mass and the neutrino mass deviation are influenced. The answer was found by the following way: Unrandomized spectra with biased energy scales were created (see (29))

$$L_{\mathrm{exp}}(T_i) = L_{\mathrm{th}}(T_i + \delta, 1.0, 1.0, Q + \delta, 0.0) \tag{49}$$

and fitted by the "correct" theoretical spectra $L_{\mathrm{th}}(T_i, R_s, R_b, Q, m_\nu)$, with δ being a constant energy scale bias and $T_i \in \{18\,545.0,\ 18\,545.5,\ 18\,546.0,\ ...,\ 18\,577.0\}$. The error ellipses method was used for spectra evaluation assuming one year measurement. The results are given in Tab. 3.

δ [V]	$\overline{m}_\nu - m_\nu$ [eV]	$\sigma^+_{m_\nu}$ [eV]
100	-1.01×10^{-5}	0.206
50	-5.55×10^{-6}	0.206
30	-3.23×10^{-6}	0.206
10	-1.05×10^{-6}	0.206

Table 3: Constant energy bias. δ is an energy scale bias, m_ν represents the initial neutrino mass, $\overline{m}_\nu$ stands for the fitted neutrino mass, $\sigma^+_{m_\nu}$ is the upper estimation on the neutrino mass deviation. Pseudoexperimental spectra (49) were evaluated by the error ellipses method. See text for details on spectra parameters

We would like to emphasize that the neutrino mass shifts are independent on the measurement time. Finally, we can conclude, that our experiment is insensitive to the biased voltmeter. It is due to the fact that the spectrum length is short and both the relative spectrum amplitude and the endpoint are fitted.

2.5.2 Step variation of energy bias

Let us assume, that our voltmetr is well calibrated, but the calibration is time unstable in the way, that the energy scale shifts. We have simplified this case in the following way: Let us "measure" a spectrum using a well calibrated and time stable voltmeter for a half of the total measurement time. After this period, let an imperfection exhibits by shifting our energy scale. Further, let us assume that we do not recognize that a failure has happened and let us continue to "measure" the spectrum for the rest of time. Then, the pseudoexperimental spectrum

$$\begin{aligned} L_{\mathrm{exp}}(T_i) &= \frac{L_{\mathrm{exp},1}(T_i) + L_{\mathrm{exp},2}(T_i)}{2} \\ L_{\mathrm{exp},1}(T_i) &= L_{\mathrm{th}}(T_i, 1.0, 1.0, Q, 0.0) \\ L_{\mathrm{exp},2}(T_i) &= L_{\mathrm{th}}(T_i + \delta, 1.0, 1.0, Q, 0.0) \end{aligned} \tag{50}$$

is fitted by the "correct" theoretical spectrum $L_{\mathrm{th}}(T_i, R_s, R_b, Q, m_\nu)$, with δ being an energy scale bias and $T_i \in \{18\,545.0, 18\,545.5, 18\,546.0, ..., 18\,577.0\}$. The spectra were evaluated by the error ellipses method assuming one year measurement. Then, the experimental spectrum deviation (31) can be expressed as

$$\sigma_{\mathrm{exp}}(T_i) = \sqrt{\frac{L_{\mathrm{exp},1}(T_i) + L_{\mathrm{exp},2}(T_i)}{2 \cdot 365.25 \cdot 24 \cdot 3600}} \tag{51}$$

χ^2 minimizers (28) were found fitting the linear neutrino mass, the neutrino mass squared deviations were investigated fitting the neutrino mass squared. The results are shown in Tab. 4.

δ [V]	$\overline{m}_\nu - m_\nu$ [eV]	$\sigma^-_{m^2_\nu}$ [eV^2]	$\sigma^+_{m^2_\nu}$ [eV^2]
1.00	−0.8017	0.0669	0.0649
0.50	−0.3765	0.0529	0.0509
0.30	−0.2203	0.0490	0.0460
0.10	−0.0718	0.0462	0.0426
0.05	−0.0358	0.0458	0.0425
0.03	−0.0218	0.0457	0.0424
0.01	−0.0050	0.0457	0.0424

Tab. 4: Step variation of energy bias. δ is an energy scale bias, m_ν represents the initial neutrino mass, $\overline{m}_\nu$ stands for the fitted neutrino mass, $\sigma^-_{m^2_\nu}$ and $\sigma^+_{m^2_\nu}$ are the upper and the lower estimations of the neutrino mass squared deviation. Pseudoexperimental spectra (50) were evaluated assuming one year measurement

Also in this case, the neutrino mass shifts are independent on the measurement time.

2.5.3 Gaussian blurred energy bias

This is another variant of the time dependent bias of the energy scale, probably the more realistic one. In this case, the time a biased spectrum is measured for is connected to the bias, and the dependence is given by the Gaussian distribution form. We fitted the pseudoexperimental spectrum

$$L_{\mathrm{exp}} = \int_{-\infty}^{+\infty} L_{\mathrm{th}}(T_i + u \cdot \delta, 1.0, 1.0, Q, 0.0) \cdot \frac{1}{\sqrt{2\pi}} \exp\left(\frac{-u^2}{2}\right) \mathrm{d}u \qquad (52)$$

by the "correct" theoretical spectrum $L_{\mathrm{th}}(T_i, R_s, R_b, Q, m_\nu)$, with δ being an energy bias deviation and $T_i \in \{18\,545.0,\ 18\,545.5,\ 18\,546.0,\ ...,\ 18\,577.0\}$. Regarding numerical calculation of (52), the integral was discretized with $0.025 \cdot \delta$ step and restricted to $(-4\delta,\ 4\delta)$ interval. The spectra were evaluated by the error ellipses method assuming one year measurement. Therefore, the experimental spectrum deviation (31) can be expressed as

$$\sigma_{\mathrm{exp}}(T_i) = \sqrt{\frac{L_{\mathrm{exp}}(T_i)}{365.25 \cdot 24 \cdot 3600}} \qquad (53)$$

The results are shown in Tab. 5. As well as in the previous case, χ^2 minimizers (28) were found fitting the linear neutrino mass, and the neutrino mass squared deviations were investigated fitting the neutrino mass squared. This choice was done, because we believe, that the neutrino mass squared deviations are more suitable for physical interpretation of nonphysical results.

δ [V]	$\overline{m}_\nu - m_\nu$ [eV]	$\sigma^-_{m^2_\nu}$ [eV^2]	$\sigma^+_{m^2_\nu}$ [eV^2]
0.50	−0.7892	0.0656	0.0640
0.30	−0.4517	0.0549	0.0531
0.10	−0.1435	0.0473	0.0434
0.05	−0.0709	0.0462	0.0425
0.03	−0.0423	0.0459	0.0425
0.01	−0.0140	0.0459	0.0424

Tab. 5: Gausian blurred energy bias. δ is a deviation of energy scale bias, m_ν represents the initial neutrino mass, $\overline{m}_\nu$ stands for the fitted neutrino mass, $\sigma^+_{m^2_\nu}$ and $\sigma^-_{m^2_\nu}$ are the upper and the lower estimations of the neutrino mass squared deviation. Pseudoexperimental spectra (52) were evaluated assuming one year measurement

Again, the neutrino mass shifts are independent on the measurement time. We found this energy scale imperfection the most crucial one.

2.5.4 Wrong slope of the calibration line

Another typical energy scale imperfection typical for a wrong calibration of a voltmeter is an imperfect slope of the calibration line. The same effect can be achieved by drifting dividing ratio of a high voltage divider. Both effects can be treated as a changed energy step (a width of energy bins).

In order to describe how this defect influences neutrino mass sensitivity, the following approach was chosen: Pseudoexperimental unrandomized spectra

$$L_{\mathrm{exp}} = L_{\mathrm{th}}(T_i', 1.0, 1.0, Q', 0.0) \tag{54}$$

were fitted by the "correct" theoretical spectrum $L_{\mathrm{th}}(T_i, R_s, R_b, Q, m_\nu)$, with δ being a relative change of energy step, $T_i \in \{18\,545.0, 18\,545.5, 18\,546.0, ..., 18\,577.0\}$ and

$$T_i' = T_i + (T_i - T_1) \cdot \delta \qquad\qquad Q' = Q + (Q - T_1) \cdot \delta \tag{55}$$

As well as in the previous cases the total "measurement" time was one year. Finally, we would like to emphasize that a time constant change of the energy step is assumed only. For the results see Tab. 6.

δ [ ]	$\overline{m}_\nu - m_\nu$ [eV]	$\sigma^+_{m_\nu}$ [eV]
1×10^{-3}	−0.1036	0.283
5×10^{-4}	−0.0729	0.266
1×10^{-4}	−0.0324	0.235
5×10^{-5}	−0.0230	0.227
1×10^{-5}	−0.0102	0.217
5×10^{-6}	−0.0072	0.215
1×10^{-6}	−0.0031	0.209

Tab. 6: Wrong slope of the calibration line. δ is a relative change of the energy step, m_ν represents the initial neutrino mass, $\overline{m}_\nu$ stands for the fitted neutrino mass, $\sigma^+_{m_\nu}$ estimates the upper neutrino mass deviation. See text for spectra parameters

Also in this case, the fitted neutrino mass shifts are independent on the measurement time.

2.5.5 Varying slope of the calibration line

The last imperfection we have examined is a time dependent modification of the previous effect. This includes time instability of both the voltmeter and the high voltage divider.

The following approach was chosen: Let us create two pseudoexperimental spectra. First, the correct pseudoexperimental spectrum and second, the spectrum with the changed energy step. Let us assume that the spectrum endpoint is the same in both cases. Then, let us mix the spectra together and fit them with the "correct" theoretical spectrum. The total measurement time was chosen to be one year and both particular parts of spectra were measured for the equal time i.e. half year each. The pseudoexperimental spectrum was derived as

$$\begin{aligned} L_{\mathrm{exp}}(T_i) &= \frac{L_{\mathrm{exp},1}(T_i) + L_{\mathrm{exp},2}(T_i)}{2} \\ L_{\mathrm{exp},1}(T_i) &= L_{\mathrm{th}}(T_i, 1.0, 1.0, Q, 0.0) \\ L_{\mathrm{exp},2}(T_i) &= L_{\mathrm{th}}(T_i', 1.0, 1.0, Q, 0.0) \end{aligned} \tag{56}$$

with $T_i \in \{18\,545.0,\ 18\,545.5,\ 18\,546.0,\ ...,\ 18\,577.0\}$ and

$$T_i' = T_i + (T_i - T_1) \cdot \delta \tag{57}$$

where δ is denoting a relative change of the energy step. The results are shown in Tab. 7. The deviations of the neutrino mass squared were estimated by the error ellipses method.

δ [ ]	$\overline{m}_\nu - m_\nu$ [eV]	$\sigma^-_{m^2_\nu}$ [eV^2]	$\sigma^+_{m^2_\nu}$ [eV^2]
1×10^{-3}	-0.0762	0.0463	0.0427
5×10^{-4}	-0.0524	0.0460	0.0425
1×10^{-4}	-0.0231	0.0457	0.0424
5×10^{-5}	-0.0165	0.0457	0.0424
1×10^{-5}	-0.0074	0.0457	0.0424
5×10^{-6}	-0.0054	0.0457	0.0424
1×10^{-6}	-0.0023	0.0457	0.0424

Tab. 7: Varying slope of the calibration line. δ is a relative change of an energy step, m_ν represents the initial neutrino mass, $\overline{m}_\nu$ stands for the fitted neutrino mass, $\sigma^-_{m^2_\nu}$ and $\sigma^+_{m^2_\nu}$ are the upper and the lower estimations of the neutrino mass squared deviation. See text for spectra parameters

As well as in all the previous cases, no dependence of the neutrino mass shifts on the measurement time was observed.

Conclusion

The aim of this work was to investigate how the possible energy scale imperfections influence neutrino mass sensitivity in the KATRIN experiment.

First, we developed a numerical model of the experiment. The integrated beta spectra were the basic elements we had worked with. These were derived with respect to differential beta spectra correspnding to four-fermion static approximation and the theoretical instrumental transmission function corrected for inelastic scattering in the source and isotropic tritium beta decay. Rotational-vibrational excitation states of the daughter molecule were considered. Two indepedent normalization methods were discussed and typical experiment parameters were set according to the last experiment proposal. The spectra were evaluated using the least squares method by varying four free parameters – the relative norm of the spectra, the relative norm of the background, the beta spectrum endpoint and the neutrino mass. The deviations of the fitted parameters were derived by two independent methods. In particular, the independent measurements method and the error ellipses method were utilized. Mathematical statistics required us to prolong the beta spectrum into nonphysical region of negative masses. Finally, the possibility to fit the neutrino mass squared was added into our model.

Then we focused on the accuracy and consistency tests. The numerical precision was found satisfying. We demonstrated that our physical prediction does not depend on whether we fit the linear neutrino mass or the mass squared. The dependence of the neutrino mass deviation on the total measurement time made evident that neutrino mass squared had been the correct physical parameter in the fits. The dependence of the neutrino mass squared deviation on the neutrino mass was shown to be constant. We studied the dependence of the neutrino mass deviation on the spectrum length and the background amplitude. The derived covariance matrices demonstrated that the correlation coefficients were independent on the manner how the neutrino mass had been fitted. Then the neutrino mass histogram enabled us to estimate the probability density function of the neutrino mass and to connect the neutrino mass deviations with apropriate confidence levels. Concerning the results, we proposed e.g. that the sensitivity on the massless neutrino for three year measurement is 0.20 eV on 90 % c. l. The dependence of the neutrino mass deviation on the spectrometer resolution was the concluding consistency test we had done.

Finally, the influence of possible energy scale imperfections on the neutrino mass was examined. We picked up typical imperfections from a broad scale of the possible ones; in particular, the energy bias and disturbed calibration line. Both static and time dependent variants were considered. We demonstrated that the experiment was completely insensitive to constant energy bias. On the other side, a dynamic modification of the previous effect, especially Gaussian blurred energy

bias was found to be the crucial energy scale imperfection in the KATRIN experiment. The study of improper calibration line showed that static variant of this imperfection contributed more to systematic error than the time dependent modification. This behaviour is the general expected one.

In conclusion, it is feasible to measure the neutrino mass with proposed sensitivity of 0.35 eV on 90 % c. l. in the KATRIN experiment. However, it seems not to be desirable to rely on electrical measurement only, but it is highly recommended to employ physical reference of electron energy.

This work was partly supported by the Grant Agency of the Czech Republic under contract No. 202/03/0889.

References

[1] A. Osipowicz et al. (KATRIN Collab.), `hep-ex/0109033` (2001)

[2] T. Thümmler et al. (KATRIN Collab.), Addendum to the Letter of Intent, KATRIN internal report (2002)

[3] V.M. Lobashev, Windowless gaseous tritium source (WGTS), KATRIN internal report (2000)

[4] B. Bornshein, KATRIN internal report *95-TRP-1303* (2002)

[5] J.D. Jackson, *Classical Electrodynamics*, Wiley, New York, 3rd edition (1999)

[6] N.A. Titov, KATRIN internal report *65-ME-4004-1* (2002)

[7] V.N. Aseev et al., Eur. Phys. J. D **10**, 39–52 (2000)

[8] A. Špalek, O. Dragoun, KATRIN internal report *95-TRP-1314* (2002)

[9] A. Kovalík, J. Electron Spectr. Relat. Phenom. **58**, 49 (1992)

[10] K. Eitel, KATRIN internal report *65-SRP-4008-1* (2002)

[11] A. Saenz et al., Phys. Rev. Lett. **84**, 242 (2000)

[12] C. Weinheimer, KATRIN internal report *65-ME-4002-1* (2002)

[13] C. Weinheimer, KATRIN internal report *95-TRP-1301* (2002)

[14] D.W.O. Rogers, Nucl. Inst. and Meth. **127**, 253–260 (1975)